THE ASTROPHYSICAL JOURNAL, 430:142–162, 1994 July 20

THE RELATIONSHIP BETWEEN PAST AND PRESENT STAR FORMATION IN GALACTIC DISKS FROM CCD SURFACE PHOTOMETRY

STUART D. RYDER[1] AND MICHAEL A. DOPITA
Mt. Stromlo and Siding Spring Observatories, Australian National University, Weston Creek P.O., ACT 2611, Australia
Received 1993 October 7; accepted 1994 January 18

ABSTRACT

We present some results of a major new multiband imaging survey of 34 nearby southern spiral galaxies. Images in V, I, Hα, and the adjacent red continuum have been obtained using a CCD and focal reducer on the 1.0 and 2.3 m telescopes at Siding Spring Observatory. Surface photometry using the GASP software package is used first to derive the disk orientation parameters, then to provide deprojected radial surface brightness profiles for each galaxy in V and I, as well as the continuum-subtracted Hα, which traces the present-day rate of massive star formation. In the outer disk, the Hα profile can be reasonably well fitted by an exponential disk, but with a scale length much *longer* than the V scale length, which itself tends to be slightly longer than the I scale length. An almost universal relationship is observed in the disk between the Hα surface brightness and the I-band surface brightness at a given radius, with any residual offset from the mean trend being a weak function of the morphological type. Thus the rate of massive star formation per unit area in the disk is closely related to the old stellar mass surface density at each radius, and to the mean H I surface density in the disk as a whole. This forms the basis for a law of (or rather, a constraint on) massive star formation in the disks of spiral galaxies, one that has a surprising degree of independence from both galactic dynamics and molecular gas content.

Subject headings: galaxies: photometry — galaxies: spiral — galaxies: stellar content — stars: formation

1. INTRODUCTION

In spite of some remarkable recent advances in fields such as infrared and submillimeter astronomy, there is surely still much to be learned about the evolution of spiral galaxies from the optical wavelength regime. One of the most fundamental and physically meaningful quantities that can be measured in nearby galaxies is the run of surface brightness (azimuthally averaged) with radius. When properly measured, surface brightness (usually expressed in magnitudes per square arcsecond through a given filter) can be related to a surface luminosity density and has the advantage that it is a distance-independent quantity. However, conversion to a surface density of total mass requires the adoption of a mass-to-light ratio, whose absolute value and variation within the disks of spiral galaxies is still not well understood. The M/L value required to fit the observed rotation curves appears to be a complex function of the galaxy mass, morphological type, and disk inclination (Kent 1986). The existence of radial color gradients complicates matters further by signalling that the stellar age distribution and metallicity, and hence the mass-to-light ratio, probably also varies with radius in the disk (see the review by Casertano & van Albada 1990).

The use of various filters to separate out the stellar populations can be particularly instructive. In nearby spiral galaxies, the Johnson V band highlights the populous A-type dwarfs of intermediate age, as well as the more evolved giants (Mattila 1980; Kennicutt 1986; Bica 1988), while the I-band filter brings out mainly the older K-type giant population (and in addition, suffers less absorption due to dust than the bluer filters). At the other extreme, narrow-band images centered on the Hα emission line at 6563 Å can be used as a quantitative tracer of the rate of massive ($\gtrsim 10\ M_\odot$), and therefore recent ($\lesssim 10^7$ yr), star formation (Kennicutt 1983, hereafter K83). To date, very little has been done to compare the results from broad-band and narrow-band surface photometry, other than the study by Kennicutt (1989, hereafter K89), who found a good 1:1 correlation between the scale lengths.

Ryder & Dopita (1993, hereafter Paper I) present Hα images for 25 galaxies, obtained as part of a major CCD imaging survey of large, nearby southern spiral galaxies, carried out using a focal reducer on both the Mt. Stromlo and Siding Spring Observatories 1.0 and 2.3 m reflectors. The aim has been to use as much as possible the same imaging setup and analysis technique throughout so that results can be compared *directly*, rather than drawing together results for a mixture of filters, telescopes, and detectors from a variety of sources in the literature. In this way, it is hoped that new observational constraints may be placed upon the plethora of star formation prescriptions proposed to date (Matteucci 1989, and references therein). The difficulty in settling upon a unique form for the star formation law seems to be related to the fact that there are as yet insufficient observational constraints, as well as the fact that the coupling with the Initial Mass Function (IMF), whose form and behaviour both within and between individual galaxies is still not adequately constrained, remains uncertain.

How then is the present-day rate of massive star formation related to the underlying old stellar population in spiral disks? Does the new star formation indeed follow the pattern of the old (and thus preserve disk scale lengths), or is it dictated instead by the present-day gas distribution, as predicted by Schmidt-type laws for star formation? In this paper we compare the Hα surface brightness at each radius in the disk with the I-band surface brightness at that same radius to see if there is a meaningful relation between the two, as well as whether such a relationship is universal across all galactic disks.

We start by reviewing the observation and data reduction

[1] Current address: Department of Physics and Astronomy, University of Alabama, Box 870324, Tuscaloosa, AL 35487.

procedures, and discuss the surface photometry analysis and flux calibration. The derived radial profiles are presented in § 3, and the inferred disk scale lengths in each filter are discussed in § 4. We demonstrate in § 5 that a universal relationship between past and present star formation in galactic disks of the type sought does in fact exist, and also consider its dependence on other factors. We close with a discussion in § 5.2 of the implications of our findings with regard to the evolution of normal disk galaxies. In a companion paper (Dopita & Ryder 1994, hereafter Paper II), we use this new observational relationship to examine critically many of the star formation prescriptions currently in vogue, and then describe a new model for star formation in galactic disks that includes a dependence on both the surface density of gas and of total mass, and that actually satisfies our observational relationship quite well.

2. IMAGE REDUCTION AND ANALYSIS

2.1. *CCD Imaging*

The sample selection criteria, imaging setup, and observational procedure have already been described in Paper I and will be reviewed only briefly here. The sample galaxies all lie south of declination $+15°$, with heliocentric velocities no greater than $+1850$ km s^{-1}. The full range of Hubble subtypes from S0 to Sm has been covered. A focal reducer was employed at the $f/18$ focus of both the 1.0 and 2.3 m telescopes in order to provide a CCD pixel scale of $1\farcs26$ pixel^{-1} and $0\farcs54$ pixel^{-1} respectively, and a usable image area (limited mainly by filter vignetting) of diameter $\sim 8'$ and $\sim 3\farcm5$ respectively. For the narrow-band imaging, three consecutive 1000 s exposures through the appropriate 15 Å bandpass Hα filter were followed by two more exposures of 500 s through a 55 Å filter centered on 6676 Å, which isolates the nearby red continuum due to foreground stars, ionizing clusters, and the unresolved stellar population. Exposures were made only under photometric conditions, and 300 s exposures of three planetary nebulae in the Large Magellanic Cloud having well-determined fluxes (Meatheringham & Dopita 1991a, b, and references therein) were obtained at least once each night to furnish an absolute Hα flux calibration.

The Hα and red continuum images were accompanied by broad-band imaging using filters virtually identical to those specified by Bessell (1990) for CCD systems: $V = 2$ mm of GG495 + 3 mm of BG39, and $I = 3$ mm of RG9 (difficulties with cementing the elements together forced the omission of the 2 mm of WG305, which serves only as a fill). Two exposures, each of 500 s, were taken per filter. Each set of galaxy images was bracketed by images of E-region standards (Graham 1982). These provided an absolute magnitude calibration, as well as a continual monitoring of the atmospheric transparency. Multiple images of the twilight sky in all filters were taken for flat-fielding the narrow-band and broad-band data.

Standard CCD reduction techniques have been performed using the CCDRED tasks within version 2.9.1 of the IRAF[2] package. All images were debiased and then flat-fielded using a master flat-field, constructed by averaging the individual, non-registered twilight flat-fields, together with a $\pm 3\ \sigma$ clipping to eliminate cosmic rays and stars. To form the final image of each galaxy in each filter, the component images were registered using foreground stars, scaled to a common mode, and then either (1) they were averaged with $\pm 3\ \sigma$ clipping (in the case of the three Hα images), or (2) the maximum value at each pixel was rejected (for the two red continuum images), or else (3) a simple averaging was used (for the two V and I images). This prevents any cosmic rays from degrading the continuum-subtracted Hα image, while the surface photometry software used is relatively immune to cosmic rays, foreground stars, and cosmetic defects in the CCD. Last, the red continuum image was sky-subtracted, registered, and suitably scaled before being subtracted from the Hα image, to yield a pure Hα line emission image.

Aperture photometry of the E-region standards, after extinction corrections, has been used to define the magnitude zero point of each broad-band galaxy image. The rms scatter between the 3–6 E-region standards available per frame was typically ~ 0.03 mag. From aperture photometry of the LMC planetary nebulae, a system sensitivity was derived based on the procedure of Jacoby, Quigley, & Africano (1987), with allowance made for the effects of ambient temperature and object redshift on the effective transmission of the Hα filters. The planetary nebulae fluxes were found to disagree consistently by some 15%, although the relative flux calibration from night to night, using a flux-weighted mean sensitivity, should still be much better than this.

2.2. *The Galaxy Surface Photometry (GASP) Package*

The GASP software package within the Starlink suite of astronomical software was chosen for the surface photometry analysis. This software, originally written by M. Cawson for the VAX/VMS operating system, has been ported to a Unix environment in order to make use of the increased speed and data handling capabilities of modern Unix-based workstations.

Preparation for the surface photometry involves, first, converting the pixel values from real numbers to integers in the range from 0 to 32,767, followed by masking out of the vignetted corner regions and bad columns in all the images (and additionally in the case of the continuum-subtracted Hα images, any incompletely subtracted stellar residuals). The sky background is determined from the modal peak of the histogram of all data values within 20 pixels of the image border. The mean sky brightness in V and I for our data set was found to be 21.0 ± 0.2 and 19.2 ± 0.3 mag arcsec^{-2}, respectively, which is in good agreement with the typical values for Siding Spring at New Moon: 21.5 and 19.3 mag arcsec^{-2}, respectively (Robinson et al. 1989). Finally, the galaxy nucleus is identified interactively, and any particularly bright stars or cosmic rays that may upset the statistical analysis are masked out with data values that will be ignored by the analysis software.

The GASP algorithm has already been described elsewhere, for example, by Davis et al. 1985 and Jedrzejewski (1987). Briefly, GASP iteratively attempts to fit ellipses of a specified semimajor axis to the galaxy image, varying the ellipticity and position angle (but in this case holding the ellipse center fixed at the position of the nucleus) so as to minimize residuals about the mode of the pixel values around the ellipse perimeter (or at larger radii, pixel values within elliptical annuli). The software uses a variation on the technique of Fourier descriptors in order to characterize the deviations from a perfect ellipse, and to identify the parameter (ellipticity or position angle) most in need of adjustment. When a satisfactory fit is

[2] IRAF is distributed by the National Optical Astronomy Observatories, which is operated by the Association of Universities for Research in Astronomy, Inc. (AURA), under cooperative agreement with the National Science Foundation.

achieved, it repeats the process for progressively larger ellipses (the semimajor axis being increased by 15% each time) until either the sky background is reached, or less than 60% of an ellipse will fit on to the image. The output file lists the optimum ellipticity and position angle for each semimajor axis, together with both the modal and the mean pixel intensities calculated in annular sectors around each ellipse. For the broad-band images, the modal intensities are best, as they are insensitive to foreground stars and cosmic rays. For the Hα images, however, it is necessary to employ the mean pixel intensities to smooth over the resolved H II regions and spiral arm structure. The last step is the conversion of the appropriate pixel intensities at each radius to absolute surface brightness, using the magnitude zero point defined by the E-region standards, and applying corrections for atmospheric plus Galactic extinction. The relative extinction in V and I was taken as $0.78A_B$ and $0.38A_B$, respectively (where A_B is the Galactic extinction in B), based on Savage & Mathis (1979) and $A_V = 3.1E(B-V)$.

To begin with, the analysis was run separately on the V and the I images of each galaxy. The resultant ellipse parameters at the 22.5, 23.0, and 23.5 mag arcsec^{-2} levels in both images were examined to decide upon the most likely inclination and position angle of the disk. The radial intensity analysis was then repeated with the ellipse parameters held fixed at these values. The resulting surface brightnesses have been "deprojected" to face-on by subtracting a geometrical factor of 2.5 log (cos i) at all radii (Boroson 1981; but see also Kent 1985, who advocates an empirical factor of 1.7 log [cos i]). In doing so, we have implicitly assumed the disk to be optically thin (but see Disney, Davies, & Phillipps 1989 for a contrary view) and dust-free. In this way, we have attempted to simulate the surface photometry that would result if we could view all the spiral disks from face-on.

After identifying the nucleus position, the same disk parameters and surface photometry procedure were applied to the continuum-subtracted Hα image (except that mean pixel intensities have been considered). The mean Hα surface brightness is defined in a manner analogous to the broad-band data, with the relative extinction at Hα of $0.64A_B$. Again, the Hα disk has been assumed to be optically thin, and the mean surface brightness as a function of radius deprojected to face-on. An Hα surface brightness zero point of +24.0 mag arcsec^{-2} has been adopted (mainly for convenience in the plotting), corresponding to an Hα flux density of 10^{-15} ergs cm^{-2} s^{-1} arcsec^{-2} reaching the top of the Earth's atmosphere. Following K83, an extra 1.1 mag mean extinction correction has been applied to the Hα fluxes so as to make some allowance for absorption by the dust internal to the H II regions themselves.

3. RADIAL SURFACE BRIGHTNESS PROFILES

The relevant parameters for each of the 34 galaxies for which a complete set of V, I, and continuum-subtracted Hα images were obtained from either the 1.0 or 2.3 m telescopes are listed in Table 1. The morphological types, optical heliocentric velocities, and isophotal major diameters D_{25} are taken from de Vaucouleurs et al. (1991, hereafter RC3), the distances R are

TABLE 1

GALAXIES IMAGED IN THIS SURVEY

Galaxy	Type	V_{hel} (km s^{-1})	R (Mpc)	i	A_B (mag)	D_{25}	Telescope (m)
NGC 45	SA(s)dm	468	5.9	43°	0.05	8.5	1.0
NGC 1187	SB(r)c	1546	16.3	42	0.00	5.5	1.0
NGC 1313	SB(s)d	446	4.5	41	0.04	9.1	1.0
NGC 1398	PSB(r)ab	1491	16.1	47	0.00	7.1	1.0
NGC 1637	SAB(rs)c	710	8.9	41	0.12	4.0	1.0
NGC 1640	SB(r)b	1643	19.1	13	0.00	2.6	2.3
NGC 1688	SB(rs)d	1223	13.5	50	0.00	1.4	2.3
NGC 1744	SB(s)d	643	7.8	66	0.00	8.1	1.0
NGC 1808	RSAB(s)a	1014	10.8	68	0.06	6.5	1.0
NGC 2217	SB(rs)0$^+$(R)	1609	19.5	23	0.14	4.5	1.0
NGC 2427	SAB(s)dm	972	10.9	72	0.73	5.2	1.0
NGC 2442	SAB(s)bc(P)	1399	17.1	62	0.70	5.5	1.0
NGC 2835	SB(rs)c	876	10.8	51	0.41	6.6	1.0
NGC 2997	SAB(rs)c	1090	13.8	47	0.51	8.9	1.0
NGC 3059	SB(rs)bc	1292	14.8	23	0.77	3.6	2.3
NGC 3115	S0$^-$(sp)	670	6.7	64	0.10	7.2	1.0
NGC 3175	SAB(s)a?	1095	14.9	78	0.24	5.0	1.0
NGC 3351	SB(r)b	771	8.1	45	0.05	7.4	1.0
NGC 3368	SAB(rs)ab	943	8.1	48	0.06	7.6	1.0
NGC 3423	SA(s)cd	835	10.9	33	0.08	3.8	2.3
NGC 3593	SA(s)0/a:	624	5.5	70	0.00	5.2	1.0
NGC 3621	SA(s)d	623	7.1	67	0.40	12.3	1.0
NGC 4192	SAB(s)ab	−126	16.8	81	0.14	9.8	1.0
NGC 4548	SB(rs)b	498	16.8	40	0.07	5.4	1.0
NGC 5068	SAB(rs)cd	537	6.7	29	0.31	7.2	1.0
NGC 5643	SAB(rs)c	1163	16.9	23	0.41	4.6	1.0
NGC 6118	SA(s)cd	1586	25.4	68	0.46	4.7	1.0
NGC 6384	SAB(r)bc	1690	26.6	46	0.41	6.2	1.0
NGC 6744	SAB(r)bc	730	10.4	47	0.11	20.0	1.0
NGC 7205	SA(s)bc	1482	20.5	60	0.00	4.1	1.0
NGC 7424	SAB(rs)cd	914	11.5	28	0.00	9.5	1.0
IC 4710	SB(s)m	741	8.9	31	0.38	3.6	1.0
IC 5201	SB(rs)cd	844	11.1	62	0.00	8.5	1.0
IC 5332	SA(s)d	706	8.4	31	0.00	7.8	1.0

from Tully (1988), and the Galactic blue extinction values A_B are from Burstein & Heiles (1984). The inclinations i are those determined from this study, and are calculated from q, the apparent minor-to-major axis ratio by

$$\cos^2 i = \frac{q^2 - q_0^2}{1 - q_0^2} \quad (1)$$

(Hubble 1926), where q_0, the intrinsic axis ratio, is taken to be 0.2 after Holmberg (1946), although it is quite likely a weak function of the morphological type (Heidmann, Heidmann, & de Vaucouleurs 1972). Figure 1 is a plot of the predicted inclinations using the axis ratios in RC3 against those derived from the GASP axis ratios. With two exceptions, the agreement is quite satisfactory. For NGC 1640, GASP derives a lower inclination than RC3 ($i = 13°$ against $i = 40°$), but a higher value for NGC 2442 ($i = 62°$ as against $i = 28°$). Tully (1988) suggests $i = 0°$ and 28°, respectively, while Lauberts & Valentijn (1989) claim $i = 59°$ and 74°, respectively, from ellipse fitting to the octants of the B-band images. While NGC 1640 has a distinctly elliptical central bar and ring, the outer arms form a loose, nearly circular ring, giving support to the lower inclination derived by GASP. The case of NGC 2442 is somewhat more complicated (Paper I). The dominance of the asymmetric arms complicates the disk orientation analysis, but by the same token casts some doubt on the usefulness of assigning a characteristic surface brightness at each radius in this particular case.

Figure 2 displays all of the deprojected surface brightness profiles as functions of radius from the galaxy center, using the distances and fixed ellipse inclinations given in Table 1. The I-band profiles (usually the uppermost ones) are marked with the symbol "I," the V profiles by a "V," and the Hα profiles by "α." Occasionally, the Hα surface brightness has dropped too close to the sky to be reliable (e.g., NGC 1637); in such cases, the points have not been plotted, and a straight line has been used instead to join the surrounding points which do have sufficient signal-to-noise. The dominant source of error is generally in the determination of the sky background. Although upwards of 30,000 pixels would be used in forming the histogram, this merely allows us to compute the mode of the border pixel intensities to a high accuracy, and still may not necessarily reflect the true sky value. Because of our limited field coverage, there is an increased bias toward overestimating the sky brightness, which would cause our profiles to curve downwards at large radii. Indeed, there is evidence in Figure 2 of such behavior in some cases, especially among the I-band profiles (where field coverage is most limited), which may be indicative of oversubtraction of the sky level. We should be wary of attaching too much significance to the outermost points.

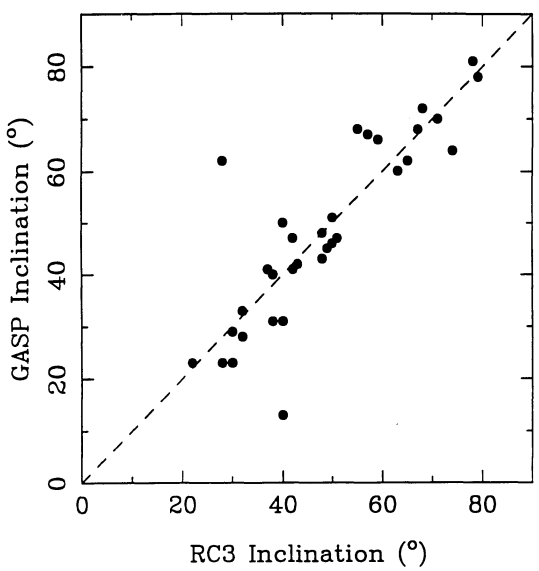

FIG. 1.—Comparison of the disk inclinations derived from major-to-minor axis ratios in RC3, and those from the GASP analysis. The dashed line indicates one-to-one correspondence.

Error bars have been left off so as not to unduly clutter the plots. The standard deviations, calculated from Gaussian fits to the pixel intensity histograms at each radius, are not good indicators of the measurement errors as such; rather they reflect the difficulties in assigning a characteristic intensity as the constrained ellipses cut across spiral arms or resolved H II regions, as well as the scatter introduced by CCD readout noise and any residual flat-fielding errors. By taking at least 40 samples per ellipse in the inner regions (using bilinear interpolation between pixels if necessary) and up to 9000 samples per ellipse in the outer disk, the true characteristic surface brightness can, in principle, be determined to a much greater accuracy than this. We show in Figure 3 the purely statistical error bars for the surface photometry of NGC 4548, calculated using an approach due to R. J. Buta (1993, private communication). In the bulge and inner disk, the dominant source of error is the residual scatter in the photometric standards; however, as the surface brightness drops below 1% of the night sky (marked by the dashed line), the error bars grow rapidly, due to the limit set by uncertainty in the sky level. By varying the width of the border strip used to construct the sky histogram, we estimate this uncertainty to be on the order of 0.5%, 0.1%, and 0.3%, respectively, for the V, I, and Hα images of NGC 4548. Although based on only one particular galaxy, Figure 3 is intended to serve as a guide to the relative uncertainty to be expected at any given surface brightness in each of the filters for the sample as a whole.

We have compared the GASP radial profiles with those produced using equivalent routines within the IRAF package. For both the broad-band and narrow-band data, the profiles exhibit quite similar behavior, and seldom differ by more than 0.2 mag arcsec^{-2}. We have also been able to compare the Hα surface photometry of NGC 1313 with an image obtained using TAURUS II and a CCD on the 3.9 m Anglo-Australian Telescope (affording better spatial resolution and an order of magnitude greater sensitivity). Despite half a magnitude or so of disagreement in the bar region, the agreement in the outer disk is seen to be very good, with many trends in the AAT data being followed closely by the 1.0 m profile. Finally, we have been able to compare our free-fitting GASP results with a similar analysis by Prieto et al. (1992) in V and I for NGC 6118. Both the optimum ellipticity and the derived surface brightness profiles are in extremely good agreement, although there does appear to be a zero-point discrepancy between the I-band results (Ryder 1993).

4. DISK SCALE LENGTHS

A close inspection of the deprojected Hα profiles in Figure 2 will show that although the majority can be fairly well fitted by exponential disks, their scale lengths are nearly always *longer* than the corresponding broad-band profiles. This contradicts the K89 result, but is in agreement with the findings of Dopita,

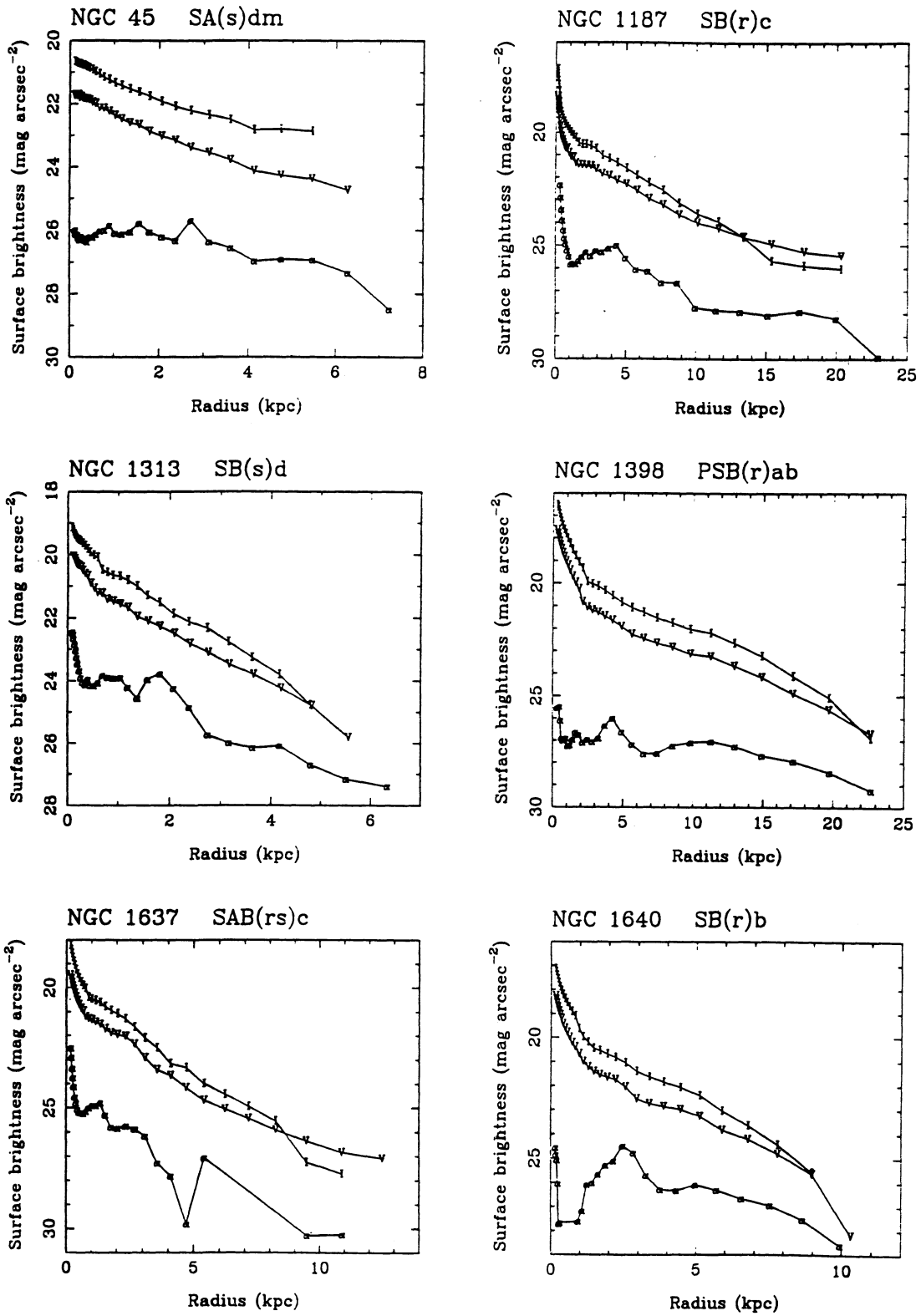

FIG. 2.—Plots of the deprojected surface brightness radial profiles for each of the 34 galaxies in our survey. The central surface brightness of NGC 3115 is so high that the *I*-band radial profile is saturated in the nucleus.

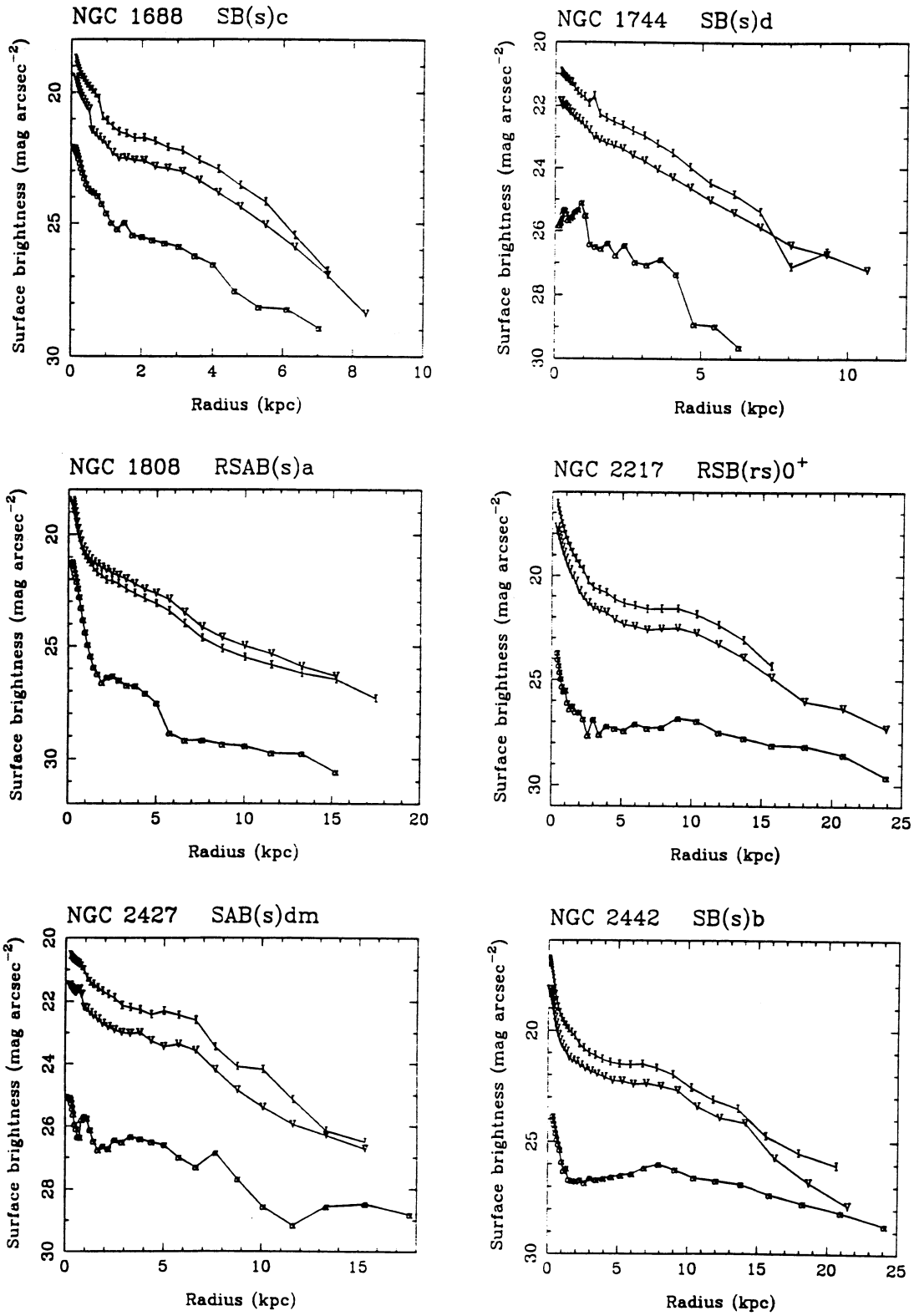

FIG. 2.—*Continued*

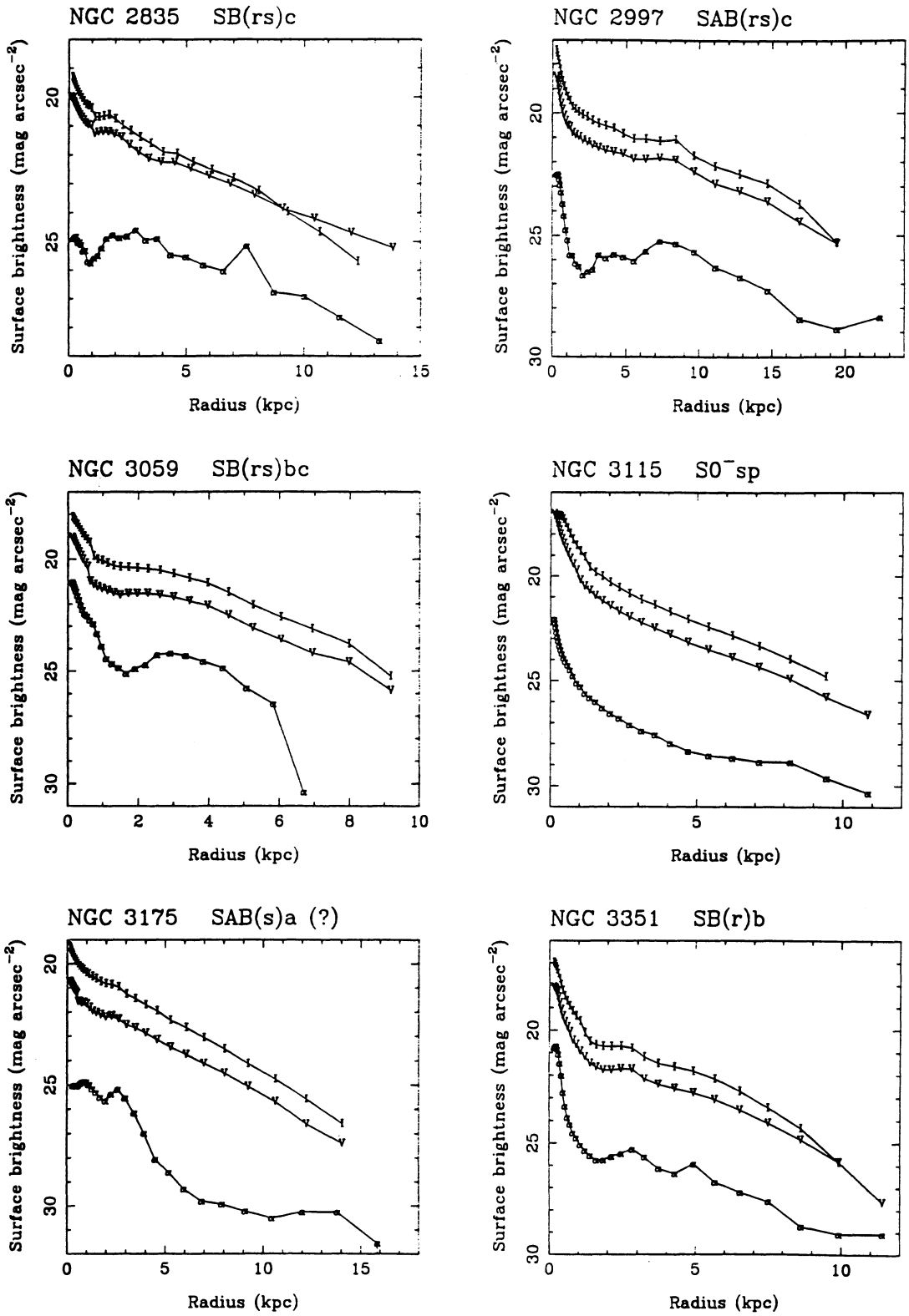

FIG. 2.—*Continued*

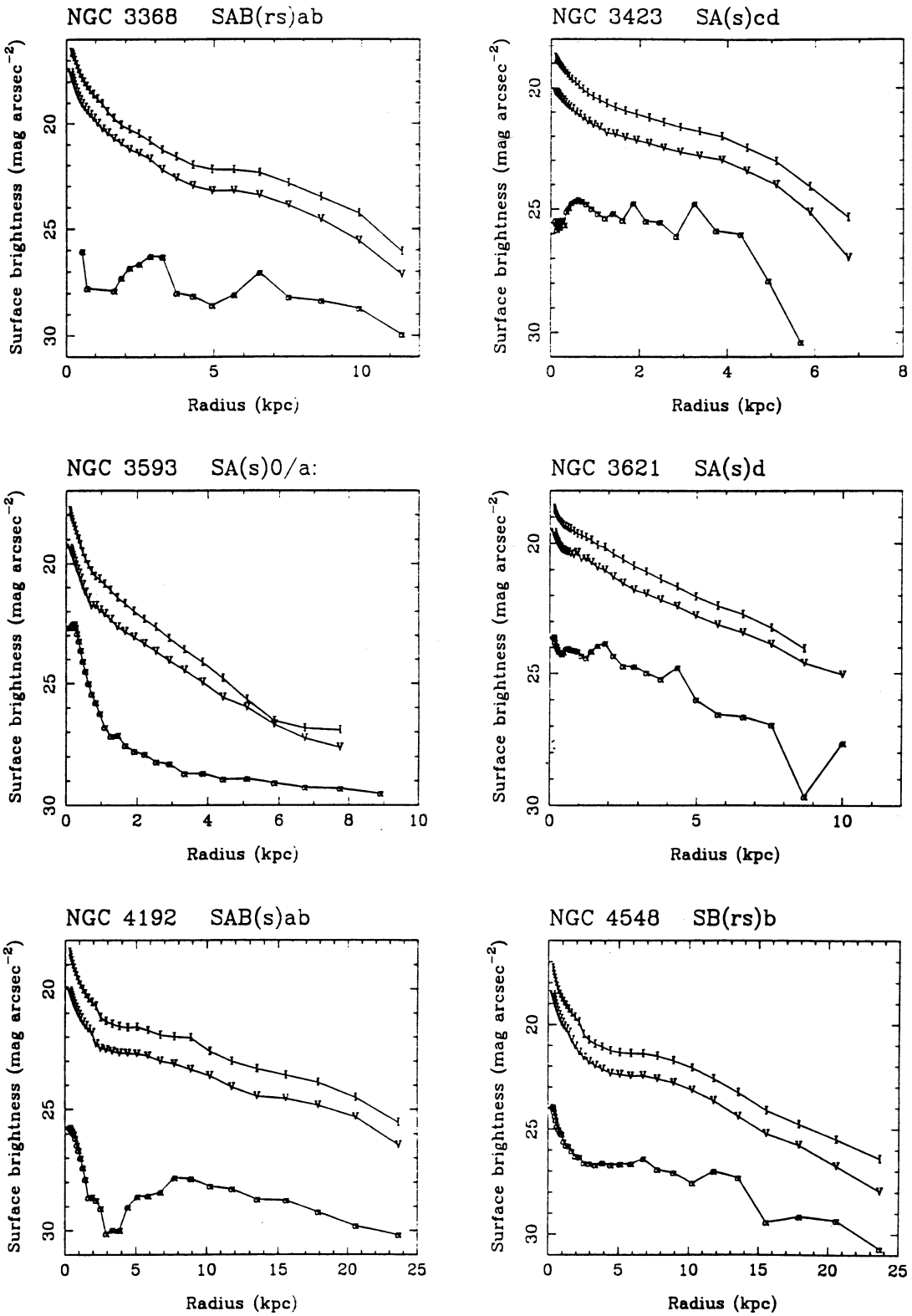

FIG. 2.—*Continued*

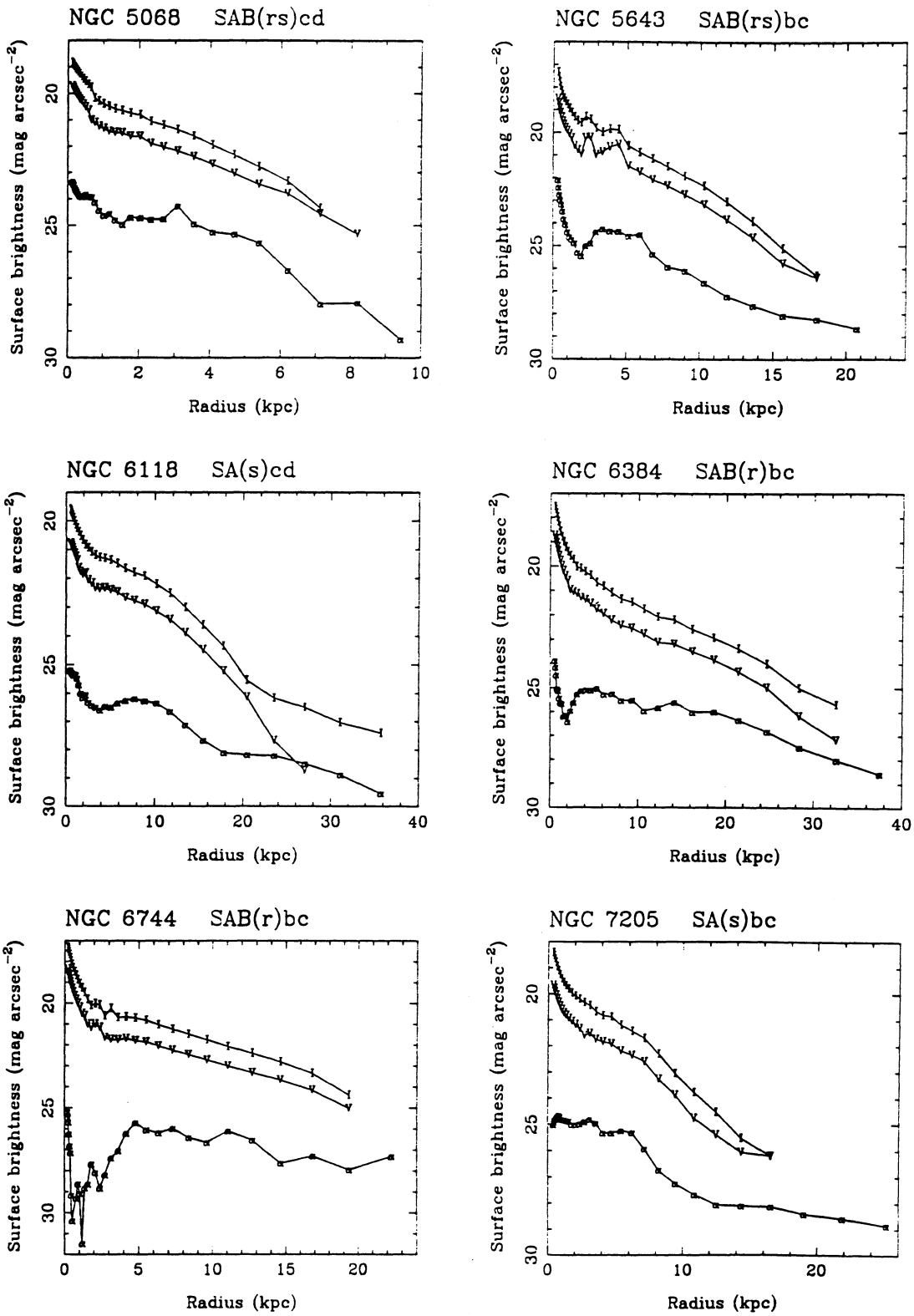

FIG. 2.—*Continued*

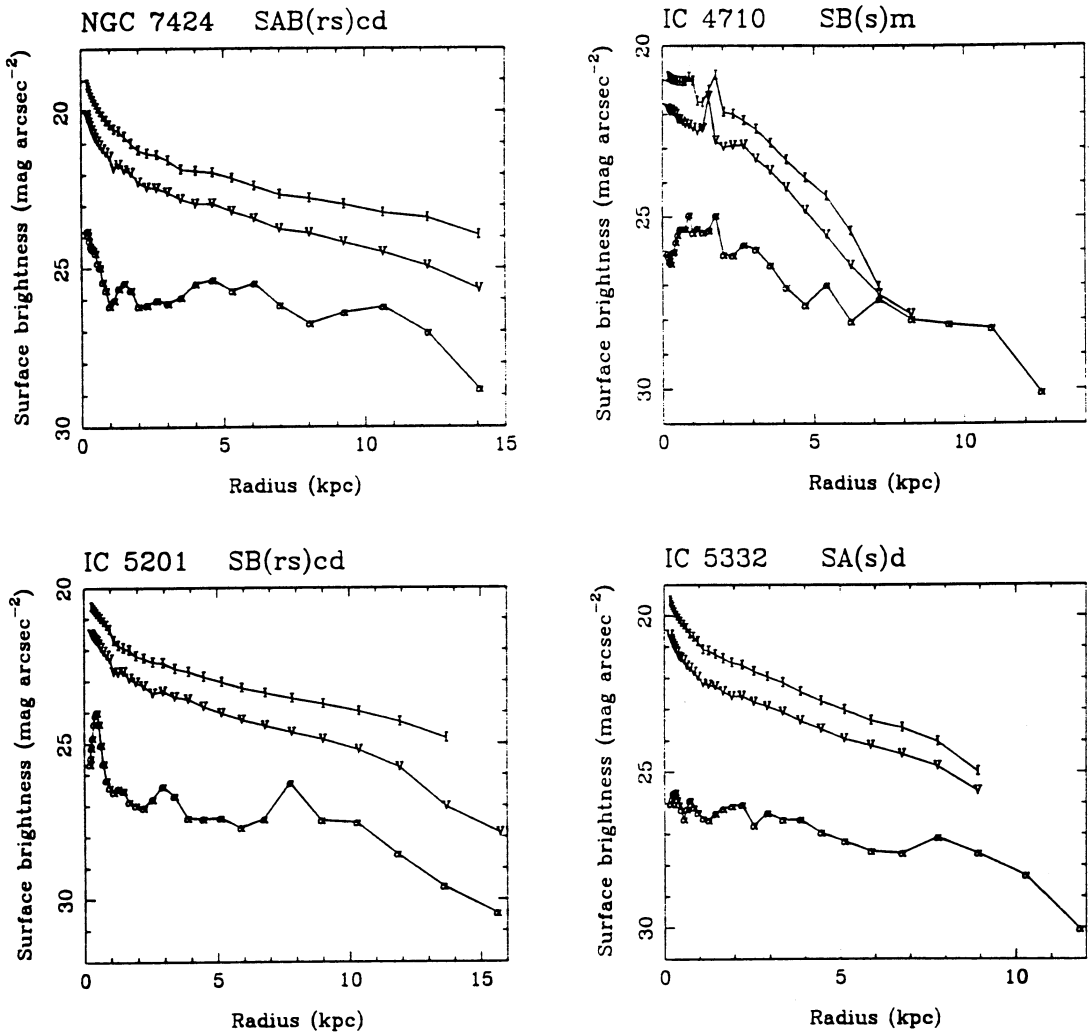

FIG. 2.—*Continued*

Forster, & Ferrario (1990) from narrow-band imaging of four southern late-type spirals. We recall that K89 in fact counted H II regions within elliptical annuli, then appealed to the apparent radial constancy of the H II region luminosity function in a number of spirals (Kennicutt, Edgar, & Hodge 1989, hereafter KEH89) to equate star formation *distribution* with star formation *rate*. The similarity in the H II region LF between the "inner" and the "outer" part of the disk has recently been confirmed in M101 by Scowen, Dufour, & Hester (1992), and in NGC 6814 by Knappen et al. (1993), although Rand (1992) noticed a difference in their slopes in the interacting spiral M51. The important point is that our technique integrates all the Hα flux in the elliptical annuli, including the diffuse component of H II emission, which can be significant, especially in the early-type galaxies and in the interarm regions.

Since this finding constitutes one of the major results of this study, it is vital that some time is devoted to validating it, and ensuring that it is not merely a systematic effect of our reduction or analysis procedures. One possibility may be that the red continuum has been oversubtracted. A constant scaling factor (0.8) was applied to the red continuum images before subtraction, and found to produce satisfactory removal of both the resolved and unresolved stellar components. However, as a check, some of the galaxies with the flattest Hα profiles were reanalyzed, this time using the Hα plus continuum image. These images often show scale lengths much more like that of the *V* and the *I* images. However, this means that the pure Hα disk must indeed have a scale length longer than that of the old stellar disk, as the relative importance of the red continuum tends to increase going toward the nucleus. The use of maximum pixel value rejection (as opposed to a simple averaging) in forming the red continuum image is not the cause of problems either since, if anything, it would tend to lead to undersubtraction of the red continuum. Our 6676/55 filter samples the red continuum immediately adjacent to the Hα line, and therefore minimizes any error due to the variation of the continuum slope around Hα, arising from the radial variation in stellar population mix implied by the existence of color gradients.

Extinction by dust is another possibility that needs to be considered. Since the *V* and *I* bands bracket the Hα line, none of the standard wavelength-dependent extinction models could explain why the Hα profile should be quite shallow while the *V* and *I* disks are quite similar. Admittedly, the two populations being imaged (stars and H II regions) have quite different scale

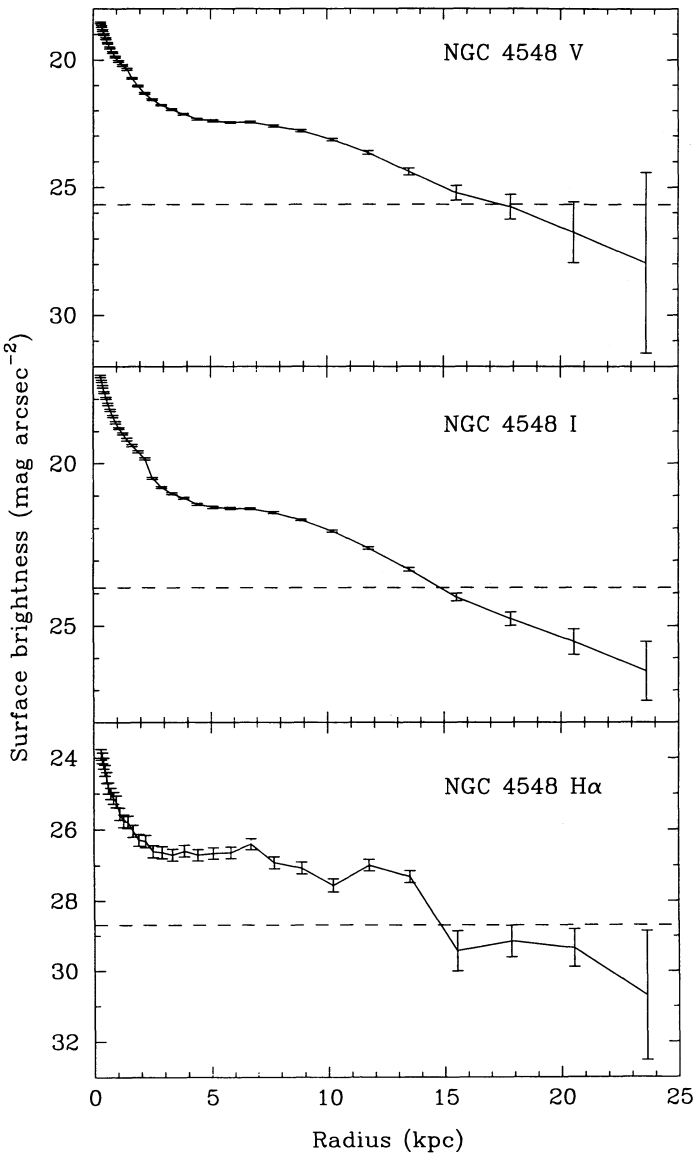

FIG. 3.—Deprojected radial surface brightness profiles for NGC 4548, with statistical error bars included. The dashed line in each plot marks the surface brightness equivalent to 1% of the night sky in that filter.

heights and thus differing levels of surrounding dust. But such a well-defined Hα disk would imply a remarkably smooth and perhaps universal radial extinction gradient, for which no clear evidence is forthcoming from combined radio and optical studies of H II regions in nearby galaxies (e.g., Kaufman et al. 1987; Israel & Kennicutt 1980). Furthermore, it will be shown shortly that there exists a well-defined relationship of the Hα surface brightness at each radius with the *I* band surface brightness *at that same radius.* Such a relationship ought to be shattered if extinction was such a dominant factor.

It is possible that comparing modal surface brightness for the broad-band data with mean surface brightness for the Hα images is not strictly valid. Since the modal Hα surface brightness is meaningless, some broad-band radial profiles using mean surface brightness values were computed instead. While this often did result in the *V* and *I* scale lengths being somewhat longer, at best it made them similar to the Hα scale lengths. Our inability to mask out every cosmic ray and foreground star in the broad-band images forces us into using the mode as our parameter of interest. But in the presence of dust lanes, ionizing clusters, and the like, the most commonly occurring surface brightness *should* be our best measure of the underlying regular stellar population.

The total error bars on each surface brightness point (Fig. 3) are certainly sufficient in principle to allow the scale lengths all to be the same. However, this would require a systematic underestimation in the inner disk, and a systematic overestimation in the outer disk. Our correction for deprojection itself cannot be directly responsible as it is just a constant offset added to all points on the profile, and is the same for each filter. Phillipps et al. (1991) and Huizinga & van Albada (1992) both argue that the disk in fact undergoes a transition from being optically thin in the outer parts, to becoming optically thick farther in. This would require us to make a radially varying deprojection correction, possibly destroying the exponential character of the Hα disk. Many of our Hα profiles show the Type II behavior (Freeman 1970), with an apparent deficit of light in the bulge-disk transition region. Phillipps et al. (1991) claim to be able to "fix up" such profiles using their absorption corrections. However, a deficit in star formation activity between the bulge and the disk is perhaps to be expected if bar-driven radial gas inflow is occurring, as is seen in most of the barred spirals in our survey (Ryder 1993).

As mentioned previously, the narrow filter bandpasses can cause problems if the central wavelength and the galaxy's redshifted Hα are not well matched, and the galaxy has a large projected rotational velocity width. In such a case, one would expect to see an apparently fainter outer Hα disk as the outermost H II regions with the most extreme velocities are carried outside the peak transmission of the filter. In fact, none of the highly inclined galaxies in our sample show this behavior, and in any case, correcting for such filter bandpass effects would again tend to lengthen further the Hα disk scale lengths.

It is customary when reducing spectra of H II regions for abundance analyses to increment the equivalent width of the Hβ line by 2 Å in order to account for the fact that the Hβ emission line sits atop a (not insignificant) Hβ absorption feature in the continuum of the ionizing stars (McCall, Rybski, & Shields 1985; Roy & Walsh 1987). The effect of underlying absorption at Hα is far less severe (Kennicutt & Kent 1983), and we have not attempted to correct for it. Although underlying Hα absorption could have an impact in regions of low Hα equivalent width (i.e., the central regions of the disk), we consider it unlikely that this could account for the flattened Hα radial profiles.

It is conceivable that contamination of K89's Hα images by one or both of the nearby [N II] lines due to his use of broader filters could explain the difference in our results, especially if radial abundance gradients cause the [N II]/Hα ratio to vary significantly with radius. By fitting radial plots of the line intensity ratios from spectrophotometry of H II regions in M101 and M33 by Smith (1975), DeGioia-Eastwood et al. (1984) found $\log$ [N II]/Hα $= -0.22 - 1.0(R/R_{25})$. The relative contribution of [N II] λ6584 in a number of spiral galaxies in which [N II] is seen to be strong (and therefore potentially a major contaminant) has been evaluated, using high-resolution long-slit spectra along their major axis kindly supplied by D. S. Mathewson. It is found that in fact the ratio [N II] λ6584/([N II] λ6584 + Hα) is remarkably constant both within and between these galaxies at ~0.3. This agrees with the diagnostic

diagrams of Evans (1986), who finds very little variation in this ratio for all but the outermost metal-poor H II regions. Since the relative contribution of [N II] λ6584 (and thus that of its counterpart at 6548 Å) is nearly constant with radius, it would have hardly any effect on the derived scale length of the Hα disk if the Hα filter was to include this line. Needless to say, it would be a bizarre coincidence indeed if the effects of [N II] contamination were to make the Hα scale length match exactly that of the broad-band disk.

Perhaps the most likely cause for the scale length differences between our Hα surface photometry and K89's H II region counts is the presence of diffuse ionized gas (also referred to as the warm ionized medium [WIM]; Walterbos 1991). Because of its low emission measure ($\sim$ a few pc cm^{-6}), the existence of this component has only recently been conclusively demonstrated even in the nearby galaxies with the advent of CCD detectors. However, it is now clear that the WIM may contribute as much as 10%–40% of the total Hα flux (KEH89; Walterbos 1991), and yet it could not be included in photographic and H II region count analyses. The emission from the WIM is observed to be strongest close to the major star-forming regions, and this, coupled with increased blending of the WIM with proper H II regions in the inner disk, may well account for an increase in the Hα flux in the outer disk over that of the H II regions alone, and an apparent flattening of the radial Hα profile. Whether the source of photoionization for the WIM is OB stars or shocks due to supernovae is still unclear; in either case, however, the WIM is an indirect tracer of massive star formation that may not have otherwise shown up in the Hα flux from H II regions alone. It is therefore important that its contribution to the disk star formation rate be included.

To summarize, then, none of the likely sources of systematic error that we can think of can explain why the Hα disk scale lengths are longer than those from the broad-band imaging (indeed, correcting for such errors would only increase the scale lengths still further), and we must conclude that this is a real effect. Systematic gradients in either the extinction or in the IMF cannot be ruled out as the cause, but for lack of any other conclusive evidence for either of these, we will shortly examine the case for an increasingly flatter radial distribution of massive star formation with time.

In order to gain a more quantitative assessment of the scale length relations, straightforward linear fits to the outer disk V, I, and Hα profiles have been made (where sufficient reliable points are available), and scale lengths R_V, R_I, and $R_{H\alpha}$ derived from these. Table 2 lists these disk scale lengths, which have measurement uncertainties based on repeatability of order 0.2 kpc. No attempt has been made at bulge-disk decomposition, as the differing geometries of the bulge and the disk, together with the presence of a bar component in many cases, makes the radial profiles in Figure 2 as derived from constrained (as against free-fitted) ellipses not strictly valid for such an

TABLE 2

DERIVED GALAXY PARAMETERS

	Nuclear SFR		Total SFR		Scale Lengths (kpc)		
Galaxy	$M_\odot$ / yr	$M_\odot$ / pc^2 Gyr	$M_\odot$ / yr	$M_\odot$ / pc^2 Gyr	R_I	R_V	$R_{H\alpha}$
NGC 45	...	...	(0.8)	(4.9)	2.2	1.9	5.2
NGC 1187	0.21	68	3.4	6.4	2.9	4.0	5.8
NGC 1313	0.06	70	1.7	15.2	1.1	1.3	1.7
NGC 1398	0.04	4	2.5	2.9	4.0	4.4	11.4
NGC 1637	0.07	48	0.6	7.0	1.5	1.8	...
NGC 1640	0.01	20	1.5	8.9	1.7	2.0	2.8
NGC 1688	0.13	169	1.0	13.7	1.5	1.5	1.6
NGC 1744	...	...	(0.4)	(2.5)	1.8	2.1	1.6
NGC 1808	0.87	96	1.4	4.3	2.5	2.7	3.2
NGC 2217	0.14	20	1.7	3.3	4.6	4.5	12.1
NGC 2427	0.02	13	1.3	4.4	3.1	3.3	4.9
NGC 2442	0.14	20	4.9	6.0	3.6	3.9	8.7
NGC 2835	...	...	4.5	11.1	2.8	3.2	3.8
NGC 2997	0.43	34	8.0	6.3	5.1	5.6	6.5
NGC 3059	0.42	368	(3.8)	(26.9)	2.0	2.1	2.2
NGC 3115	0.18	56	0.5	4.0	1.7	1.8	3.1
NGC 3175	...	...	1.2	2.9	2.3	2.5	1.6
NGC 3351	0.75	93	2.1	8.5	2.1	2.3	2.4
NGC 3368	...	...	0.6	2.3	2.2	2.0	6.8
NGC 3423	...	...	(1.2)	(11.5)	1.9	2.1	3.7
NGC 3593	0.19	36	0.3	5.3	0.9	1.1	2.5
NGC 3621	...	...	(5.1)	(16.3)	2.0	2.2	2.4
NGC 4192	0.06	8	(2.0)	(1.2)	5.8	6.5	7.8
NGC 4548	0.20	16	2.1	3.6	3.8	3.6	5.1
NGC 5068	...	...	2.9	16.0	1.9	2.2	2.2
NGC 5643	0.57	63	7.9	15.8	2.8	3.1	3.9
NGC 6118	...	...	5.3	4.7	4.2	4.6	10.7
NGC 6384	...	...	20.8	9.7	5.8	6.1	10.5
NGC 6744	...	...	(6.8)	(4.3)	5.0	5.7	8.5
NGC 7205	...	...	4.5	9.6	2.3	2.5	3.8
NGC 7424	0.09	27	(4.5)	(7.3)	5.0	4.3	7.5
IC 4710	...	...	(1.3)	(2.6)	1.5	1.5	2.4
IC 5201	0.07	23	1.7	2.8	5.3	4.2	6.3
IC 5332	...	...	1.0	3.3	2.4	2.6	5.4

analysis. Furthermore, the reduced sampling and larger error bars in the disk compared with the bulge will almost certainly favor the bulge component in any attempt to fit simultaneously both an $r^{1/4}$ function to the bulge and an exponential to the disk. In addition, it is unclear whether anything more than a simple exponential fit to the radial Hα profiles is warranted. Examination of published bulge-disk decompositions (e.g., Boroson 1981; Kent 1985; Schombert & Bothun 1987) indicates that the fitted disk is never flatter than an inwards extrapolation of the outer few disk points, except in a few bulge-dominated cases, where the $r^{1/4}$ bulge function returns to dominate at large radii. Thus, the broad-band scale lengths in Table 2 are most likely upper limits to those of the pure disk components.

Photographic *B* and *I* surface photometry of three galaxies in our sample is presented in Elmegreen & Elmegreen (1984, hereafter EE84). Qualitatively at least, our *I*-band profiles are similar to their plots. When transformed to our distances, the EE84 *I* scale lengths are 1.6 kpc (NGC 1637), 10.0 kpc (NGC 6384), and 6.5 kpc (NGC 7424). Given the curvature in the *I* profiles for the latter two galaxies, the disagreement is perhaps not too surprising, except that our scale lengths are generally shorter, that is, steeper profiles. Although the aim was to have some overlap with previous Hα studies, only one of our survey galaxies has a published radial Hα profile. Hodge & Kennicutt (1983, hereafter HK83) published a smoothed, deprojected H II region relative density profile for NGC 2835. Although not one of the better fits to an exponential, HK83 quote an Hα scale length for NGC 2835 of 3.2 kpc, slightly shorter than our own value of 3.8 kpc. This is consistent with our finding that Hα disk scale lengths are in fact somewhat longer than previously believed on the basis of H II region number counts.

Figure 4 plots both the *V* and Hα scale lengths (R_V and $R_{H\alpha}$) as a function of the *I*-band scale length R_I. R_V is seen to scale linearly with R_I, but tends nearly always to be longer (i.e., a flatter profile) by ~0.2 kpc. The Hα disks display a much greater scatter, but have scale lengths on average 75% longer than the disk in *I*. As a check (to first order) whether the difference in scale lengths is due to extinction, the ratio of R_V to R_I has been plotted versus the galaxy's inclination, as suggested by Byun (1992). An increase in R_V relative to R_I with increasing inclination might be expected simply on the basis of an increasing path length through the dust, especially in the inner disk. Instead, Figure 5 displays merely a scatter, with no apparent trend, indicating once again that extinction is not systematically affecting our analysis.

Clearly then, our results indicate that the Hα radial luminosity profile slopes are *not* correlated in a one-to-one fashion with the broad-band luminosity profile slopes, contrary to the findings of K89. Very little is yet known about the spatial and temporal behavior of the IMF in disk galaxies. At the present epoch however, the *I*-band (and to a lesser extent, the *V*-band) imaging is expected to be dominated by evolved stars (Mattila 1980) rather than recently formed objects. In his spectrophotometric atlas of integrated galaxy spectra, Kennicutt (1992) shows the results of dividing spectra for various classes of spirals by a "mean" E-S0 galaxy spectrum. These indicate that the *V* filter is rather insensitive to any ongoing star formation overlying an existing old red population, with not more than ~20% or so of the total *V* luminosity being contributed by active star formation, even at such late types as Sm (the models of Huchra 1977 predict a similar fractional contribution). Although these atlas spectra do not extend beyond 7100 Å, it is

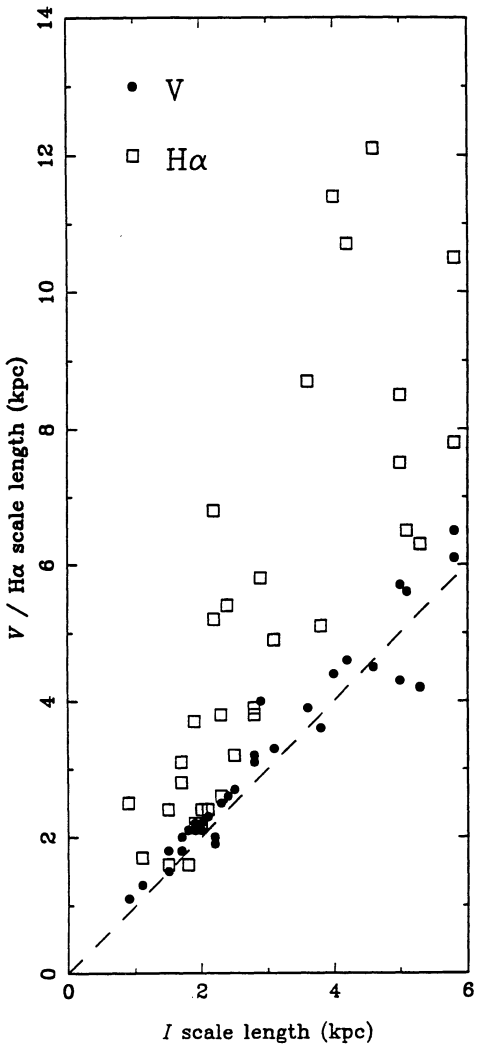

FIG. 4.—*V*-band and Hα disk scale lengths plotted against the respective *I*-band scale length. The dashed line has a slope of unity.

apparent from other sources, such as population synthesis (e.g., Charlot & Bruzual 1991), that recent star formation would make even less of a contribution to the *I* band. Thus, the current set of data does not permit us to say anything about possible radial variations in the present-day IMF, or to disentangle this from other possible effects.

The close similarity in the H II region luminosity functions for the inner and outer regions of spiral galaxies (KEH89; Scowen et al. 1992) does give us reason to think that the IMF also should not alter significantly between these two regions. If this is the case, then these scale length disparities would be telling us more about the temporal evolution of the large-scale star formation pattern in galactic disks. In particular, the increasing flatness of the radial profiles as one goes to bluer wavelengths (e.g., in M31 [Walterbos & Kennicutt 1988], and in NGC 628 [Natali, Pedichini, & Righini 1992]), but with the Hα profile being flattest of all, would be consistent with an overall increase in scale length with each new stellar population. Why this should be the case is not clear just from these data alone. Schmidt-type laws would predict that the distribution of recent star formation should follow that of the atomic or molecular gas components (or some combination thereof).

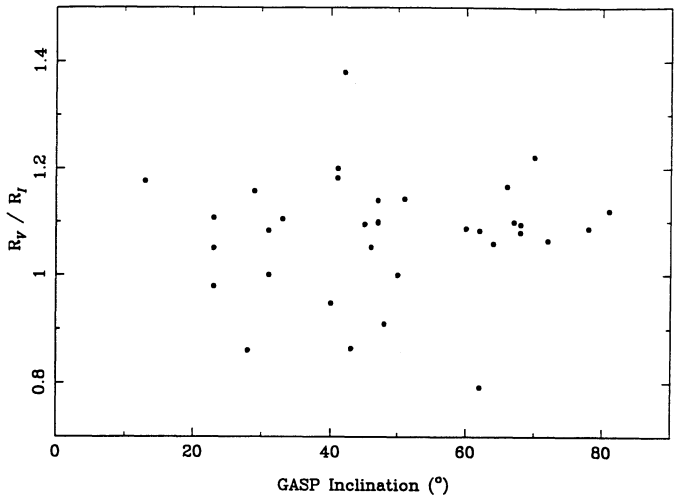

FIG. 5.—Ratio of V to I scale lengths as a function of the disk inclination determined by GASP.

Examination of radial H I profiles for several spirals of various types (e.g., Wevers 1984, hereafter W84) reveals a relatively flat distribution across the star-forming disk in virtually all cases. Thus a Schmidt Law for the *atomic* gas (even one with a power-law index $n > 1$) could give rise to a radial Hα profile of slope intermediate between that of the H I and the old stellar disk. It is notable that the molecular gas component also appears to take on an exponentially decreasing radial distribution, but with a scale length that is perhaps *shorter* than either the total or stellar mass distribution (Wang 1990b). This does, however, assume that the CO:H_2 conversion factor does not change even though the mean gas metallicity decreases with increasing radius. With all this uncertainty, and lacking much of the gas data with which to test this scenario, we can only speculate. What is clear however is that it may no longer be acceptable to characterize the various exponentially distributed components of a galactic disk (old stars, new stars, radio continuum, CO, etc.) by a *single* value of the scale length parameter.

5. A CORRELATION BETWEEN STELLAR SURFACE BRIGHTNESS AND STAR FORMATION ACTIVITY

We now move on to the main goal of this paper, a direct comparison of the past and present star formation activity in galactic disks. Because our interest is mainly in studying star formation in the disk component alone, our analysis will be restricted to those regions considered to be disk-dominated. Close examination of the deprojected radial surface brightness profiles (Fig. 2) leads us to believe that fainter than $\mu_I \sim 21$ mag arcsec^{-2}, one is fairly safe in assuming that any bulge contribution is negligible. Note that the zero point of the Hα surface brightness scale was chosen arbitrarily such that +24.0 mag arcsec^{-2} equates to an Hα flux density of 10^{-15} ergs cm^{-2} s^{-1} arcsec^{-2} reaching the top of the Earth's atmosphere.

Figure 6 consists of plots, for each galaxy and for each sampled radius in that galaxy, of the deprojected Hα surface brightness against the deprojected I-band surface brightness *at that radius*. In the few cases where the sampled radii differed for the two profiles, linear interpolation has been used. A linear least-squares fit to the *entire* set of data points yields the relation

$$\mu_{H\alpha} = (0.64 \pm 0.37)\mu_I + (12.5 \pm 7.3)\,, \qquad (2)$$

where the uncertainties have been derived from least-squares fits to each of the 34 individual curves in Figure 6. The mean value of the correlation coefficient from each of the individual fits is $R^2 = 0.8$. The mean relation described by equation (2) is plotted as the dashed line in each of the individual plots in Figure 6. Clearly, individual galaxies conform to such a correlation, but each has a different constant of star formation activity over all radii that results in an offset above or below the mean trend. In Paper II we develop the idea that some of the residual structure in these curves can be attributed to variations in the ratio of disk age to star formation efficiency, perhaps through continuous gas infall and/or discrete episodes of accretion.

Rather than attempt to normalize all of the curves at a particular value of μ_I, an offset has been estimated for each galaxy so as to minimize their overall dispersion about the mean relation. Applying these offsets to the curves of the individual galaxies (in the sense that a negative offset makes the $\mu_{H\alpha}$ values *brighter*) leaves us with the mean relation described by the compound set of curves shown in Figure 7. The overall correlation coefficient for the entire set of $\mu_{H\alpha}$ versus μ_I points is a respectable $R^2 = 0.73$, and rms scatter in $\mu_{H\alpha}$ about the mean relation is only of order 0.5 mag. Such a tight correlation over some 5 mag in μ_I (two orders of magnitude in luminosity density), and over the entire range of spiral types, is quite remarkable, and to the best of our knowledge has not previously been recognized in the literature. By using distance-independent quantities, many selection effects and spurious correlations are avoided (Lequeux 1988). Note that the slope of the compound curve is inconsistent with a slope of unity that would be expected if the Hα and I-band disk scale lengths were to be equal, confirming the result of § 4.

In order to identify what the "second parameter" in this correlation that scales the star-forming activity equally at all radii in individual galaxies might be, the required vertical offset values have been plotted against all of the other parameters available to us for each of these galaxies. One of the most promising and physically reasonable trends is one with the Hubble subtype, shown in Figure 8. This plot indicates that up to about type Sbc, the Hα surface brightness is *fainter* than it ought to be compared with the later type spirals. This can be understood as the early-type galaxies being less active in their massive star formation activity. This result is to be expected and is evidenced by their having fewer and fainter H II regions overall than the later types (KEH89). Also in Figure 8, indicated by a dashed line, is our interpretation of the underlying trend with Hubble subtype. The sizes of the points in Figure 8 are proportional to the disk inclinations, with edge-on disks having the largest point sizes. There is the suggestion here also of a correlation of the residuals with disk inclination, with the more highly inclined galaxies being slightly fainter in Hα than a face-on spiral of the same type. This is perhaps to be expected from our simplistic corrections for extinction and disk projection; however, such a trend is marginal, and swamped by the dominant behavior with Hubble subtype. Note that our simple geometrical deprojection factor, appropriate or not, is independent of the filter used and acts only to shift the profiles in Figures 6 and 7 parallel to the mean relation of equation (2).

But what is the underlying parameter that causes such a variation with Hubble subtype? We propose that it is the mean H I surface density within the disk that dictates the "base level" of star formation activity across the disk. Unfortunately, aperture synthesis maps that would allow us to determine a

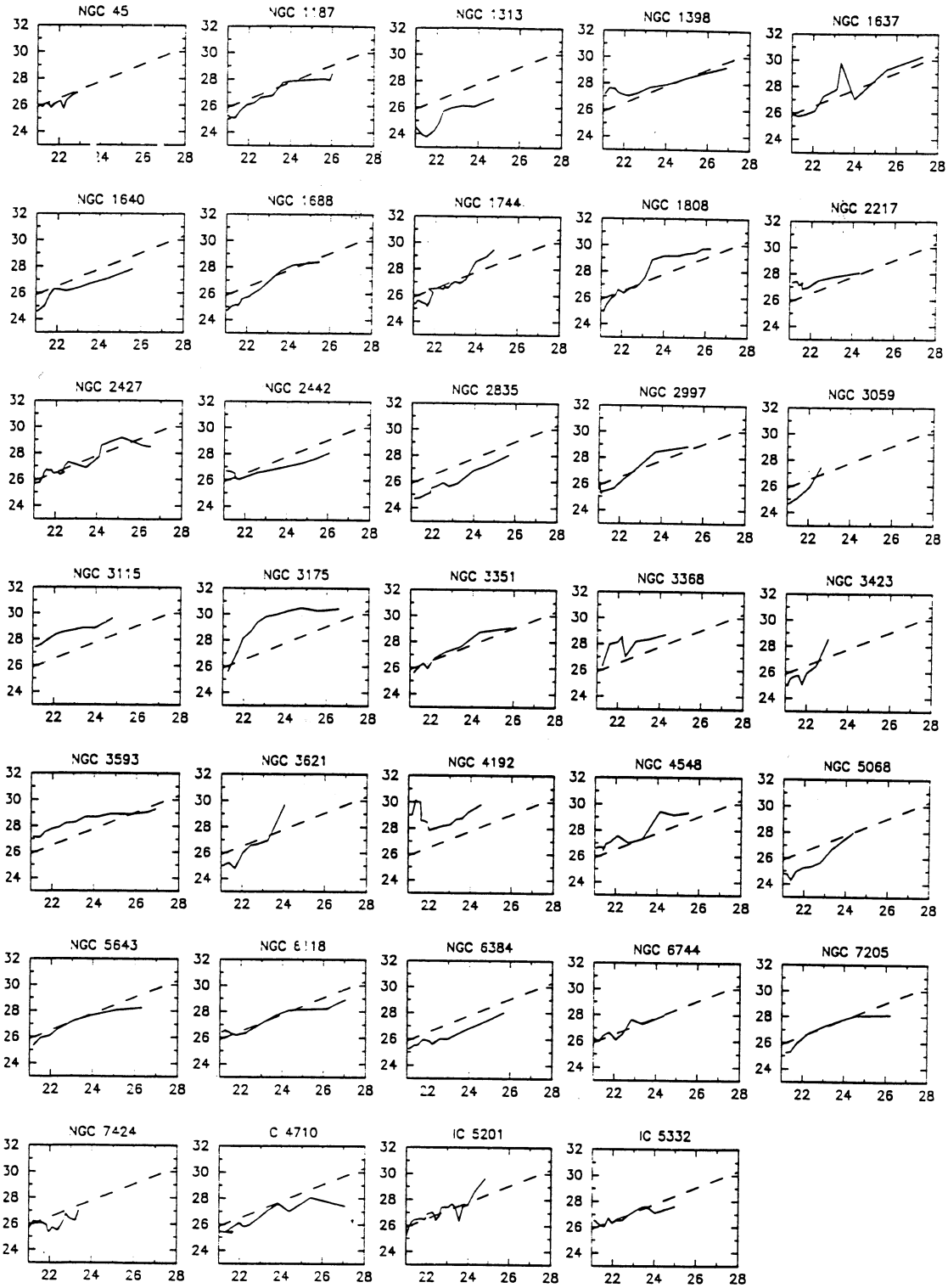

FIG. 6.—Plots of Hα surface brightness vs. the *I*-band surface brightness at that same radius, for each of the 34 galaxies in our sample. The dashed line in each plot is the fit to the entire set of curves given by eq. (2).

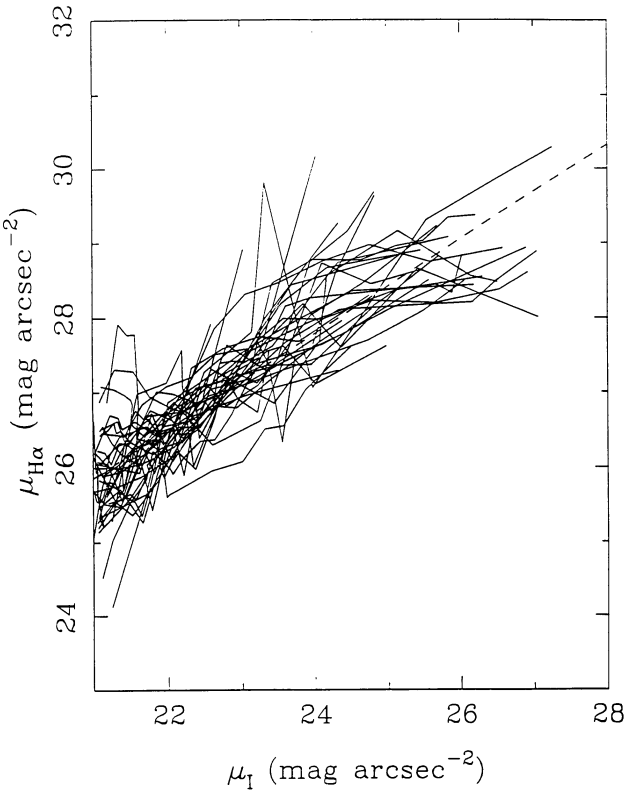

FIG. 7.—Individual curves from Fig. 6 overlaid on the least-squares fit (*dashed line*), after applying vertical offsets.

characteristic H I surface density in the star-forming disk are only available for four of the galaxies in our sample. Instead, the total H I mass M_{HI} normalized by the area of the optical disk $A_{opt} = \pi(D_{25}/2)^2$ (where D_{25} is the isophotal major diameter at the 25.0 B mag arcsec^{-2} level) will be adopted as a first guess at the true mean H I surface density. Such data have been

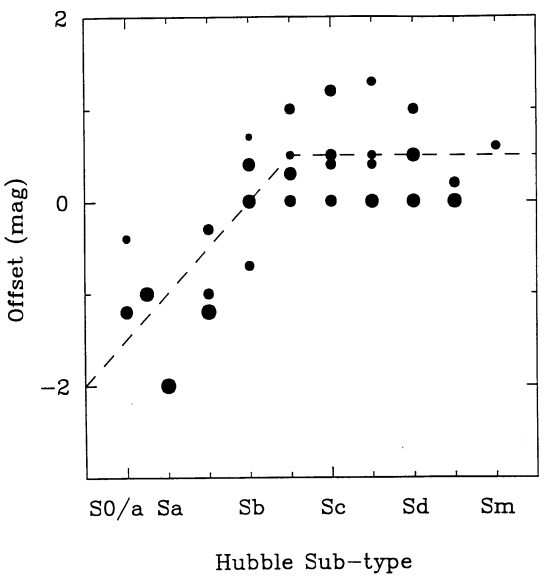

FIG. 8.—Required vertical offsets to be added to $\mu_{H\alpha}$ to make each of the individual curves in Fig. 6 match the mean relation in Fig. 7, plotted as a function of Hubble subtype.

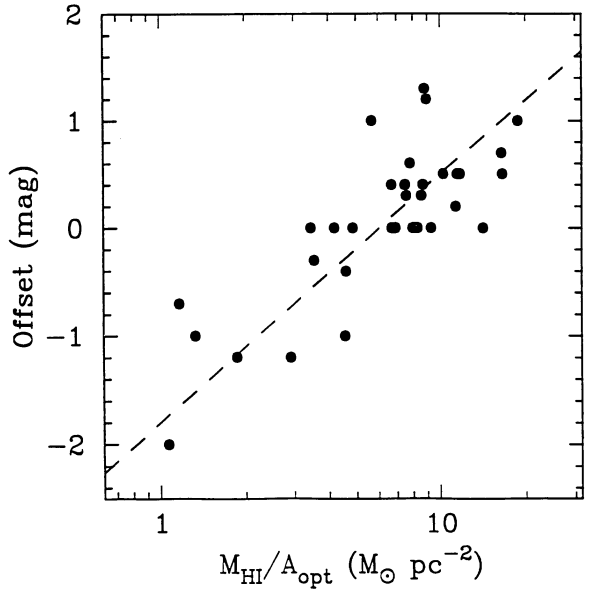

FIG. 9.—Plot of the "mean" H I surface density (integrated H I mass normalized by the area of the optical disk) vs. the offset parameter defined in Fig. 8.

compiled using the homogeneous database of Parkes 21 cm observations by Reif et al. (1982), which uses multiple pointings as necessary for the largest galaxies, together with the distances and optical diameters in Table 1. The resulting plot versus the Hα offset parameter defined above (Fig. 9) does indeed show a surprisingly tight correlation, despite the ad hoc nature of our H I surface density parameter. The linear least-squares line of best fit in Figure 9 has been determined by considering separately first the offset, then the mean H I surface density, as the independent parameter. The result is a line of slope 2.3 ± 0.5 in what is effectively a log-log plane.

Bosma (1981) finds quite a large dispersion in the ratio of H I extent to optical diameter, but no apparent trend with Hubble subtype. The four galaxies for which radial H I profiles are currently available have relatively constant surface density within the optical radius, then decline rapidly in a virtually exponential manner beyond this. Characteristic H I surface densities $\bar{\sigma}_{HI}$ have been estimated within the star-forming disk from these radial profiles and are compared with the H I surface densities used for Figure 9 in Table 3. With the exception of the anomalous NGC 1313 (which has an extended asymmetric low surface brightness envelope; Ryder et al. 1994), the integrated H I mass normalized by the optical area turns out to be quite a reasonable estimator of the true H I surface density within the star-forming disk. As with the optical

TABLE 3

MEAN AND OBSERVED H I SURFACE DENSITIES IN SAMPLE GALAXIES

GALAXY	H I SURFACE DENSITY ($M_\odot$/pc^{-2})		H I REFERENCE
	M_{HI}/A_{opt}	$\bar{\sigma}_{HI}$	
NGC 1313.....	18.8	8	Ryder et al. 1994
NGC 3368.....	4.6	4	Warmels 1988a
NGC 4192.....	2.9	2	Warmels 1988a
NGC 4548.....	1.2	1	Warmels 1988a

surface brightnesses, the H I surface density has the advantage of being a distance-independent quantity.

Figure 9 also provides some reassurance that the relationship between I and Hα surface brightness is neither severely affected by, nor the direct result of, an inappropriate extinction correction. The correlation is in the sense that the spirals most deficient in Hα emission have the lowest H I surface densities in their disks. But according to the conventional assumption that an increased column density of H I is always associated with an increased dust content, then the lack of Hα in the early-type galaxies must be intrinsic, and not due to increased absorption by dust (see also Oey & Kennicutt 1993). Conversely, the fact that the gas-rich disks shine through even more brightly in Hα indicates that dust is not having a major impact on either of the correlations presented in Figures 7 and 9. This is perhaps not too surprising since, as Bosma et al. (1992) have recently demonstrated, even edge-on spirals can be quite transparent at Hα in their outer parts.

5.1. *Calibration*

Having established that there is in fact an almost universal relationship between Hα surface brightness and I-band surface brightness at a given radius both within and between spiral galaxies, let us now move on to consider the implications and possible origins of such a relationship. By definition

$$\mu_{\mathrm{H}\alpha} \sim -2.5 \log \frac{F_{\mathrm{H}\alpha}}{\mathrm{arcsec}^2} \tag{3}$$

$$\sim -2.5 \log \frac{L_{\mathrm{H}\alpha}}{\mathrm{parsec}^2}, \tag{4}$$

where $F_{\mathrm{H}\alpha}$ and $L_{\mathrm{H}\alpha}$ are the Hα flux and luminosity, respectively. In either case, $\mu_{\mathrm{H}\alpha}$ is a distance-independent quantity. Following K83, the latter form can be equated to a rate of massive star formation per unit area, and thence to a total rate per unit area integrated over all stellar masses via an appropriate form of the IMF. Thus the Hα surface brightness in effect measures the present-day rate of star formation per unit area in the disk.

Similarly, the I band surface brightness can be related to a surface luminosity density Σ_I by

$$\Sigma_I(L_\odot\ \mathrm{pc}^{-2}) = 10^{-0.4(\mu_I - \mu_{I\odot})}, \tag{5}$$

where $\mu_{I_\odot}$ is the I-band surface brightness of 1 $L_\odot$ pc^{-2} = 25.63 I mag arcsec^{-2}. The actual conversion to a surface *mass* density, however, requires one to impose a value for the mass-to-light ratio. It is quite likely that the mass-to-light ratio is a function of (among other things) the passband used, morphological type, and distance from the nucleus (Kent 1986; Casertano & van Albada 1990; Bosma & van der Kruit 1979). For the time being we will continue working with observable quantities, but for the purposes of modeling (Paper II), this difficulty will eventually have to be confronted.

Since both $\mu_{\mathrm{H}\alpha}$ and μ_I are related logarithmically to surface mass densities, the relationship between the two given by equation (2) can be expressed as a power law between the area-specific star formation rate $\dot{\Sigma}_*$ and the surface I luminosity density Σ_I:

$$\dot{\Sigma}_* \sim (\Sigma_I)^{0.64 \pm 0.37}. \tag{6}$$

Since it seems unlikely that new stars form from the old stars (at least not directly), one cannot lay claim to this being the definitive "law" of star formation in spiral disks. What it does represent, however, is part of an important new *constraint* that must be satisfied in the long term by any prospective star formation law, whatever form that may take.

The relationship in equation (6) above will now be put on a more quantitative basis. Folding in the dependence on Hubble subtype T (as tabulated in RC3) outlined in Figure 8 gives

$$\mu_{\mathrm{H}\alpha} = 0.64\mu_I + \begin{cases} 14 - 0.5T & T < 4 \\ 12 & T \geq 4 \end{cases}. \tag{7}$$

What equation (7) allows us to do is predict a disk Hα flux, and thus a star formation rate (SFR), on the basis of I-band surface photometry, and morphological type alone. A disk SFR has been calculated by integrating the Hα flux at radii for which $\mu_I > 21$ mag arcsec^{-2}, correcting for atmospheric, Galactic, and 1.1 mag of internal extinction as well as the effective filter transmission, and then using the prescription of K83 to convert the integrated luminosity to a total SFR. The conversion formula in equation (7) has then been used to convert μ_I at the same radii to the equivalent $\mu_{\mathrm{H}\alpha}$ and a disk SFR determined from this also. A comparison of the results is shown in Figure 10, in which the dashed line has unity slope and is not an explicit fit to the data. This technique of disk SFR estimation appears to work quite well, certainly within the factor of 2 or so uncertainty associated with any value of an absolute SFR derived from Hα data on account of the variable correction for internal extinction. It is significantly more reliable than the more often used broad-band colors, and has the advantage that imaging in a single broad-band filter only is required. Given the somewhat tedious nature of narrow-band imaging, this in itself is quite a bonus, but of course one then lacks the azimuthal distribution of star formation. It must be stressed, however, that this relationship *holds only in the disks of spirals* and cannot presently be extrapolated reliably to the galaxy as a whole.

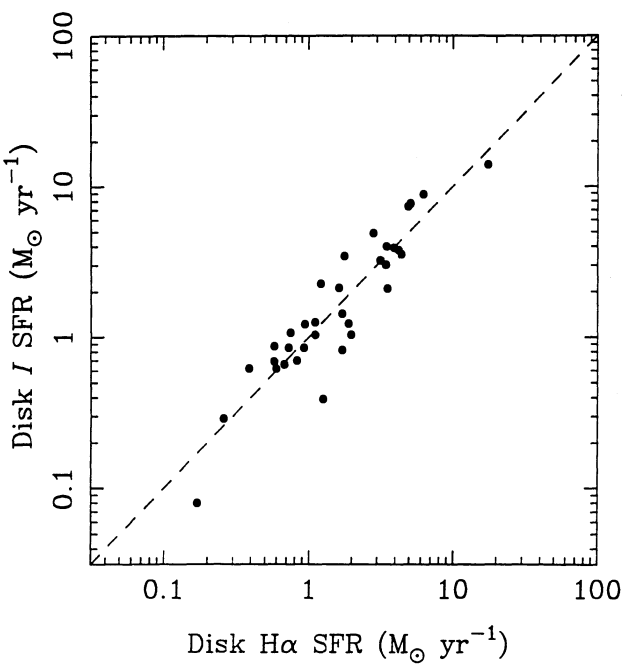

FIG. 10.—Comparison of the *disk-only* total SFRs derived from the radial Hα profiles with those derived from the I-band profiles using the conversion formula in eq. (7).

Alternatively, if a measurement of the H I content is available, one may make use of the relation in Figure 9 to substitute H I surface density $M_{\rm H\,I}/A_{\rm opt}$ or $\bar{\sigma}_{\rm H\,I}$ for morphological type. Thus

$$\mu_{\rm H\alpha} = 0.64\mu_I + 12.5 - \text{Offset}$$
$$= 0.64\mu_I - (2.3 \pm 0.5)\log(M_{\rm H\,I}/A_{\rm opt}) + (14.3 \pm 0.4)\,. \quad (8)$$

Reverting back to surface densities and using the definitions (4) and (5), equation (6) can now be supplemented with the power-law dependence on the *global* mean H I surface density $\bar{\Sigma}_{\rm H\,I}$ implied by equation (8):

$$\dot{\Sigma}_* \propto (\bar{\Sigma}_{\rm H\,I})^{0.9\pm0.2}(\Sigma_I)^{0.64\pm0.37}\,. \quad (9)$$

That is, the radial variation of the specific SFR is fixed by that for the *I*-band surface brightness, while the normalization at each radius depends almost linearly on the mean galactic H I surface density. We have used the mean ratios of molecular to atomic gas compiled as a function of morphological type by Young & Knezek (1989) in order to estimate the molecular and total gas surface densities in each of the survey galaxies. The total gas surface density shows a somewhat poorer correlation with the Hα offset parameter than does the atomic gas surface density alone, while the derived molecular gas surface density shows virtually no correlation. Thus, the H I does appear to be a useful (if not the fundamental) tracer of the raw material for massive star formation, and allows us to go some way toward studying and predicting SFRs without needing to consider the molecular component at all.

It may well be that it is in fact the local H I surface density at each radius that normalizes the rate, as predicted by some Schmidt-type laws of star formation. But since this quantity is relatively constant across the disk (e.g., W84; Warmels 1988a, b), the global mean H I surface density serves almost as well. Once again, it should be emphasized that the relation (9) holds only in the disks of spiral galaxies and is an observational constraint on the present-day rate of massive star formation only, not necessarily the definitive law of star formation over the galactic lifetime.

By chance, our choice of zero-point is such that $\mu_{\rm H\alpha} = 25$ mag arcsec^{-2} corresponds to $\dot{\Sigma}_* = 25\ M_\odot\ {\rm pc}^{-2}\ {\rm Gyr}^{-1}$ using the formula in K83, and our own particular flux calibration. Consequently, it is possible to provide a more generally useful direct calibration of $\dot{\Sigma}_*$ ($M_\odot\ {\rm pc}^{-2}\ {\rm Gyr}^{-1}$) in terms of μ_I and T:

$$\log \dot{\Sigma}_* = -0.26\mu_I + \begin{cases} 5.8 + 0.2T & T < 4 \\ 6.6 & T \geq 4 \end{cases}, \quad (10)$$

or in terms of μ_I and H I surface density:

$$\log \dot{\Sigma}_* = -0.26\mu_I + 0.92\log(M_{\rm H\,I}/A_{\rm opt}) + 5.3\,. \quad (11)$$

At any particular radius, equations (10) and (11) may give values of $\dot{\Sigma}_*$ differing by up to 0.5 mag from that predicted by the actual value of $\mu_{\rm H\alpha}$ at that radius, but integrated over the whole disk, the discrepancies should roughly even out.

Finally, each of the offset points in Figure 7 has been divided into 0.5 mag bins in μ_I, and a mean value of $\mu_{\rm H\alpha}$ computed (along with its standard deviation) for each bin. Using the fact that $\mu_{\rm H\alpha} = 25.0$ in our system corresponds to a surface luminosity density in Hα of 1.42 $L_\odot\ {\rm pc}^{-2}$, together with equation (5), allows us to plot this binned form of equation (6) on the luminosity-luminosity plane (Fig. 11). The range of the data plotted in Figures 6 and 7 has been extended to brighter and fainter surface brightness in order to see just how far equation (6) can be pushed. The relation does appear to be linear with the prescribed slope all the way from 2 to 200 $L_\odot\ {\rm pc}^{-2}$ in *I*. At the lowest surface brightness, the relation appears to be flattening off, although the effects of sky subtraction (§ 3) and small number statistics leave this open to question.

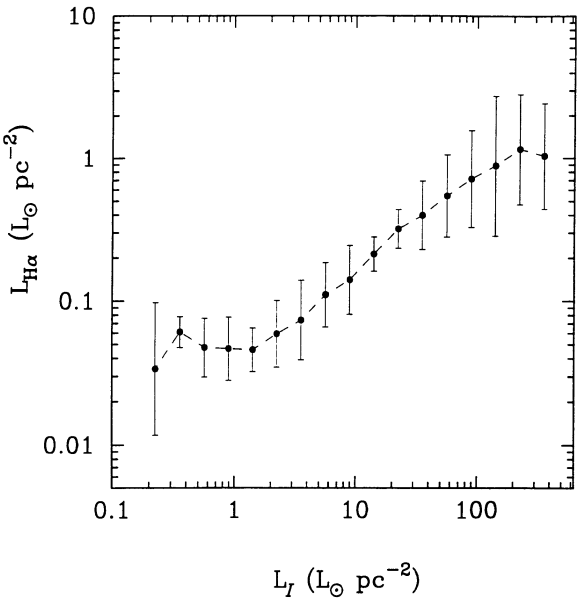

FIG. 11.—Observed relationship between surface density of Hα luminosity and *I*-band luminosity in galactic disks, after scaling to account for the variation in gas content. The error bars are $\pm 1\ \sigma$ in the variation of $\mu_{\rm H\alpha}$ in each 0.5 mag bin of μ_I.

For a model galaxy of type close to Sb (or equivalently, a model galaxy with a mean H I surface density of $\sim 5\ M_\odot$ pc^{-2}), Figure 11 is the type of relation (lacking until now) that must be satisfied eventually if the model is to be considered realistic. Constraints on other galaxy types can be placed simply by scaling Figure 11 in Hα luminosity in order to account for the variation in mean gas surface density. We take up this challenge ourselves in Paper II.

5.2. *Implications and Limits of the Star Formation Law*

One remarkable aspect of our SFR "law" is its apparent independence from dynamical effects. This is in part related to the universality of exponential Hα disks in spiral galaxies, regardless of whether the individual H II regions that are the dominant source of Hα photons are tightly confined to well-defined spiral arms (as in grand-design spirals), or distributed chaotically (as in flocculent spirals). This leads naturally to the concept of a fixed "quota" of star formation at each radius in the disk, with the spiral density waves relegated mainly to an organizational role. The nontrivial outcome of exponential Hα radial profiles from discrete sites of massive star formation is discussed more fully by Ryder (1993).

One weakness of our "law" is that it breaks down at early epochs—it cannot form any stars unless stars are already present in the galaxy! Perhaps the true form of the star formation law contains at least two components, but only that which depends on the present stellar mass density is important in the disks of spiral galaxies today. Thus, it should be some parameter that diminishes with time, or is related to some other quantity that does. Based on evidence for spatially distinct

regions of low-mass and high-mass star formation in disks, Larson (1986) and Wyse & Silk (1987) propose a bimodal formalism for star formation, the net effect in each case being an enhanced rate of massive star formation at early epochs relative to that of low-mass stars. This relieves many other problems faced by galaxy evolution theory (e.g., the need for continuous gas infall, short gas consumption timescales, the blueness of some galaxies, etc.) and could well provide the necessary "kick-start" to star formation needed to enable the observed long-term relationship in equation (9). Alternatively, it may be that the radial variation of Σ_I is today merely a convenient observational tracer of some other physical parameter, such as total mass surface density, or perhaps molecular gas surface density, in which case no kick-start may be necessary, as the truly fundamental component is presumably present when the first generation of stars formed.

Any star formation law primarily dependent upon the stellar surface density will have great difficulty in reproducing the observed age-metallicity relationship (Twarog 1980; Carlberg et al. 1985), which shows a rapid initial growth and only a slow increase of the metallicity ever since. A law of the form given simply by equation (6) would predict a runaway growth in the massive star formation rate (and thus the metallicity) as the stellar surface density continues to grow. Instead, the fact that the index of the gas component in equation (9) is numerically greater than that of the stellar component should help overcome this problem. Assuming (as most models do) a rapid early infall rate of gas onto the disk, the metallicity will also initially build up quickly. At later epochs, gas infall may be negligible, and the gas supply will diminish rapidly as the ever-increasing stellar surface density starts to dominate the SFR law. Overall, however, one expects the SFR will start to decline, and the metallicity increase to slow, due to the dominance of the gas term in equation (9). Conceivably, this could continue until either a critical gas density is reached, or perhaps until mass loss from evolved objects (e.g., planetary nebulae) ends up providing the bulk of the gas supply. The latter eventuality could at least account for a functional dependence of the SFR on the stellar surface density of old stars. Assuming then that the "priming" problem mentioned earlier can be overcome, equation (9) is in principle capable of accounting for the behavior of the observed age-metallicity relation.

Alternatively, the increasing stellar surface density may act to suppress any further star formation occurring, and thereby act as a self-regulating mechanism. While supernovae may well play a role in triggering further star formation, they are equally capable of disrupting star-forming regions. Dopita (1985) has outlined the likely role of the older stellar population in pressurizing the interstellar medium (principally through Type I supernovae), and thereby influencing the star formation rate. Thus, it is hypothesized that a combination of the declining gas supply and increasing surface density of stars is modifying the rate and distribution of star formation and results in a relationship of the form in equation (6) at the present epoch in galactic disks. These issues are addressed in a more quantitative fashion in Paper II using computer models.

Recall also that strictly speaking, the Hα flux traces only the formation of massive stars. The I-band surface brightness on the other hand ought to be related to the integral of the SFR (as measured by $\mu_{H\alpha}$) over the last 5–15 Gyr or so. Because of this, μ_I should eventually take on a 1:1 relationship with $\mu_{H\alpha}$. Thus, either the exponent in equation (6) has not always been at its present value of 0.64, or else the IMF varies with radius such as to allow more high-mass star formation in the outer disk relative to low-mass stars at the current epoch. Since neither the V nor the I-band filters are particularly sensitive to recent low-mass star formation (§ 4), the latter possibility cannot be properly addressed. One could perhaps argue that a variation in μ_I with massive SFR would arise naturally if the I-band filter was in some way sensitive to recent star formation. However the lack of any prominent emission lines or continuum features in the 7000—9000 Å range, combined with the greater range in μ_I than that in $\mu_{H\alpha}$, virtually rules out this possibility.

Another question that must be asked is why our "law" also breaks down in the bulge region of spiral galaxies. With the exception of the nuclear hot-spot galaxy NGC 1808, the individual $L_{H\alpha}$ versus L_I loci that go into making up Figure 11 all tend to flatten off at the highest surface mass densities, and display a significantly increased scatter. Although only very limited kinematical information is available for the galaxies in our sample, one can ask for example whether a transition in the rotation curve, from relatively constant velocity in the outer disk to a generally linear decline in the inner disk and bulge, could influence our star formation "law." Zaritsky (1992) has recently pointed out that an apparent change in slope in the abundance gradient of oxygen in spirals is often associated with this turnover point in the rotation curve. Such a trend is in fact predicted by the star-forming viscous disk model of galactic evolution (Lin & Pringle 1987; Sommer-Larsen & Yoshii 1989, 1990).

Alternatively, the change in slope and increased scatter in our law may reflect an underlying change in the available gas supply. Ryder (1993) shows how apparently bar-driven gas inflow can promote a central peak of star formation (and thus Hα surface brightness) in a number of these spirals, but only at the expense of that which would otherwise occur in the disk. A gas deficiency in the bulge/disk transition region would suppress the Hα luminosity, while the older stellar distribution (which suffers different forms of dispersion and diffusion over generally longer timescales than the gas) could be comparatively normal. Central "holes" in the radial H I distribution are not uncommon (e.g., Bosma 1978; W84; Warmels 1988a, b). Even in spiral galaxies without a bar, the presence of a massive spheroidal bulge can establish a turbulent shear viscosity through cloud-cloud interactions (Lynden-Bell 1969; Icke 1979) that results in the outward transfer of angular momentum and the slow radial inflow of gas (Sanders 1979; Wang 1990a). Such a mechanism could redistribute the gas in the bulge region such as to cause varying degrees of detriment to our Hα versus I-band surface brightness relationship there.

As mentioned previously, spatially resolved rotation curves either from optical or radio observations are still lacking for the vast majority of these southern spirals, even after the epochal survey of Mathewson, Ford, & Buchhorn (1992). Nevertheless, their survey data can still be used to examine whether or not the turnover radius corresponds, for example, to some characteristic value of the I surface brightness. From a sample of spirals having comparatively well-defined turnover radii, one finds a range in deprojected surface brightness at those radii of $\mu_I = 20.0$–24.0 mag arcsec^{-2}. This result is perhaps to be expected, as the less-luminous galaxies have a shorter disk scale length on average, so that for a constant central surface brightness, the $I = 21.0$ mag arcsec^{-2} isophote will be reached at a *smaller* radius than for the brighter galaxies; whereas the results of Buchhorn (1992) suggest that the

turnover radius tends to be *larger* in the lower luminosity galaxies. It should be noted that the Mathewson et al. sample is deliberately biased toward highly inclined spirals, for which our deprojection correction may be breaking down; even so, it does not appear as though disk *rotational* dynamics are a significant factor in determining the region of validity of our star formation law. One cannot, however, rule out the possible influence of motions perpendicular to the plane of the disk, which does after all possess a nonnegligible thickness. The three-dimensional structure of the disk will be considered in more detail in Paper II.

Finally, we should mention that just about any parameter or function that shows a roughly exponential decline with radius in the disks of spiral galaxies could have been substituted for Σ_I in the various figures and equations contained in this paper, and a correlation with star formation activity may still have resulted. For example, one could use the difference between the local angular frequency and the spiral pattern speed (Wyse 1986), a function of the form $(A/r - B)$ (Seiden, Schulman, & Elmegreen 1984), or even the epicyclic frequency (K89). This is not to say that the stellar surface density is probably not relevant to the star formation process; Paper II describes a model that satisfactorily accounts for Figure 11, and in which the stellar surface density is a fundamental parameter. Rather, we have used the *I*-band surface brightness throughout for its convenience, and in lieu of the missing kinematic and molecular gas data. Whatever the Hα to *I*-band correlation is telling us, it is certainly worthy of further investigation.

6. SUMMARY

Surface photometry from wide-field CCD imaging of a sample of 34 nearby southern spiral galaxies has been performed, as part of an investigation into the global rates and radial distribution of star formation in galactic disks. No previous work has obtained such uniform broad-band and narrow-band imaging (which has allowed us to compare directly the results) for such a large sample. Many of our findings challenge those obtained previously from large-aperture photometry and individual case studies.

Our first major finding concerns the relative disk scale lengths seen in the three filters. The Hα disk is moderately well represented by an exponential disk, but with a scale length much greater than that of the *V*-band disk, which itself tends to be slightly shallower than the *I*-band disk. After considering various possible systematic errors, and uncertainties in the corrections for dust and optical depth, we are led to the conclusion that these scale length differences are indeed real, especially since radial broad-band color gradients are not an uncommon phenomenon. While it had been thought up until now that the Hα disk scale lengths were similar to those in the broad-band filters, our results are in conflict with this, and suggest instead that recent massive star formation is occurring with a flatter radial mean distribution than previous stellar generations.

We have demonstrated the existence of a remarkable and almost universal correlation in the disk between the Hα surface brightness and the *I*-band surface brightness at a given radius. Thus the rate of formation of massive stars in the disk is closely related to the surface density of old stars already formed there. The loci of Hα versus *I* surface brightness have a mean slope of 0.64 ± 0.37, with most exhibiting an offset above or below the mean trend. This offset is shown to be related to the total H I mass per unit area of the optical disk, and thus presumably reflects the mean surface density of H I in the star-forming disk. Consequently, one finishes up with a "law" for predicting the present-day rate of massive star formation given by $\bar{\Sigma}_* \propto (\bar{\Sigma}_{\rm H\,I})^{0.9\pm0.2}(\Sigma_I)^{0.64\pm0.37}$. Although this formula bears some resemblance to the standard Schmidt Law for star formation, it includes an extra term dependent on the mass surface density, and is notable for its independence from galactic dynamics and molecular gas content. We caution also that this is not necessarily the definitive form of the star formation law; rather it serves simply as an observational constraint that must be satisfied in the disk at the present epoch by galaxy evolution models.

Generally, this study highlights the promise of multiband and multibandpass CCD imaging in reassessing traditionally held beliefs about the relative distributions of new and old stellar populations in spiral galaxies. Since many of these beliefs from the basis for the constraints imposed on galaxy evolution models, it is essential that we continue to hold them up to scrutiny while seeking out any new clues that may emerge from such surveys. Even tighter constraints on the various galaxy evolution scenarios must await either gas distributions for the southern spirals, or equivalent surface photometry to ours for those northern spirals already having them.

We thank S. Meatheringham and M. Buchhorn for much assistance with the GASP software. It is a pleasure to thank R. Buta, K. Freeman, M. Gregg, W. Keel, R. Kennicutt, J. Lequeux, D. Mathewson, J.-R. Roy, and the referee, R. Wyse, for many useful comments that helped strengthen the content of this paper. S. D. R. acknowledges the support of an Australian National University Postgraduate Scholarship.

REFERENCES

Bessell, M. S. 1990, PASP, 102, 1181
Bica, E. 1988, A&A, 195, 76
Boroson, T. 1981, ApJS, 46, 177
Bosma, A. 1978, Ph.D. thesis, Univ. Groningen
———. 1981, AJ, 86, 1825
Bosma, A., Byun, Y.-I., Freeman, K. C., & Athanassoula, E. 1992, ApJ, 400, L21
Bosma, A., & van der Kruit, P. C. 1979, A&A, 79, 281
Buchhorn, M. 1992, Ph.D. thesis, Australian National Univ.
Burstein, D., & Heiles, C. E. 1984, ApJS, 54, 33
Byun, Y.-I. 1992, Ph.D. thesis, Australian National Univ.
Carlberg, R. G., Dawson, P. C., Hsu, T., & VandenBerg, D. A. 1985, ApJ, 294, 674
Casertano, S., & van Albada, T. S. 1990, in Baryonic Dark Matter, ed. D. Lynden-Bell & G. Gilmore (Dordrecht: Kluwer), 159
Charlot, S., & Bruzual, A. G. 1991, ApJ, 367, 126
Davis, L. E., Cawson, M., Davies, R. L., & Illingworth, G. 1985, AJ, 90, 169
DeGioia-Eastwood, K., Grasdalen, G. L., Strom, S. E., & Strom, K. M. 1984, ApJ, 278, 564
de Vaucouleurs, G., de Vaucouleurs, A., Corwin, H. G., Buta, R. J., Paturel, G., & Fouqué, P. 1991, Third Reference Catalogue of Bright Galaxies (New York: Springer) (RC3)
Disney, M., Davies, J., & Phillipps, S. 1989, MNRAS, 239, 939
Dopita, M. A. 1985, ApJ, 295, L5
Dopita, M. A., Forster, J. R., & Ferrario, L. 1990, in The Interstellar Medium in External Galaxies: Summaries of Contributed Papers, ed. D. Hollenbach & H. Thronson (NASA CP-3084), 331
Dopita, M. A., & Ryder, S. D. 1994, ApJ, 430, 163 (Paper II)
Elmegreen, D. M., & Elmegreen, B. G. 1984, ApJS, 54, 127 (EE84)
Evans, I. N. 1986, Ph.D. thesis, Australian National Univ.
Freeman, K. C. 1970, ApJ, 160, 811
Graham, J. A. 1982, PASP, 94, 244
Heidmann, J., Heidmann, N., & de Vaucouleurs, G. 1972, MmRAS, 76, 121
Hodge, P. W., & Kennicutt, R. C. 1983, ApJ, 267, 563 (HK83)

Holmberg, E. 1946, Medd. Lunds Obs. II, No. 117
Hubble, E. 1926, ApJ, 64, 321
Huchra, J. P. 1977, ApJ, 217, 928
Huizinga, J. E., & van Albada, T. S. 1992, MNRAS, 254, 677
Icke, V. 1979, A&A, 78, 21
Israel, F. P., & Kennicutt, R. C. 1980, Astrophys. Lett., 21, 1
Jacoby, G. H., Quigley, R. J., & Africano, J. L. 1987, PASP, 99, 672
Jedrzejewski, R. I. 1987, MNRAS, 226, 747
Kaufman, M., Bash, F. N., Kennicutt, R. C., & Hodge, P. W. 1987, ApJ, 319, 61
Kennicutt, R. C. 1983, ApJ, 272, 54 (K83)
———. 1986, in Stellar Populations, ed. C. Norman, A. Renzini, & M. Tosi (Cambridge: Cambridge Univ. Press), 125
———. 1989, ApJ, 344, 685 (K89)
———. 1992, ApJS, 79, 25
Kennicutt, R. C., Edgar, B. K., & Hodge, P. W. 1989, ApJ, 337, 761 (KEH89)
Kennicutt, R. C., & Kent, S. M. 1983, AJ, 88, 1094
Kent, S. M. 1985, ApJS, 59, 115
———. 1986, AJ, 91, 1301
Knapen, J. H., Arnth-Jensen, N., Cepa, J., & Beckman, J. E. 1993, AJ, 106, 56
Larson, R. B. 1986, MNRAS, 218, 409
Lauberts, A., & Valentijn, E. A. 1989, The Surface Photometry Catalogue of the ESO-Uppsala Galaxies (Garching: European Southern Observatory)
Lequeux, J. 1988, in Millimeter and Submillimetre Astronomy, ed. R. D. Wolstencroft & W. B. Burton (Dordrecht: Kluwer), 249
Lin, D. N. C., & Pringle, J. E. 1987, ApJ, 320, L87
Lynden-Bell, D. 1969, Nature, 223, 690
Mathewson, D. S., Ford, V. L., & Buchhorn, M. 1992, ApJS, 81, 413
Matteucci, F. 1989, in Evolutionary Phenomena in Galaxies, ed. J. E. Beckman & B. E. J. Pagel (Cambridge: Cambridge Univ. Press), 297
Mattila, K. 1980, A&AS, 39, 53
McCall, M. L., Rybski, P. M., & Shields, G. A. 1985, ApJS, 57, 1
Meatheringham, S. J., & Dopita, M. A. 1991a, ApJS, 75, 407
———. 1991b, ApJS, 76, 1085
Natali, G., Pedichini, F., & Righini, M. 1992, A&A, 256, 79
Oey, M. S., & Kennicutt, R. C. 1993, ApJ, 411, 137
Phillipps, S., Evans, R., Davies, J. I., & Disney, M. J. 1991, MNRAS, 253, 496
Prieto, M., Longley, D. P. T., Perez, E., Beckman, J. E., Varela, A. M., & Cepa, J. 1992, A&AS, 93, 557
Rand, R. J. 1992, AJ, 103, 815
Reif, K., Mebold, U., Goss, W. M., van Woerden, H., & Siegman, B. 1982, A&AS, 50, 451
Robinson, R. D., Sadler, E. M., Barton, J. R., & Straede, J. O. 1989, User's Guide to CCD Detectors at the AAT (AAO UM 17.1), 14
Roy, J.-R., & Walsh, J. R. 1987, MNRAS, 228, 883
Ryder, S. D. 1993, Ph.D. thesis, Australian National Univ.
Ryder, S. D., & Dopita, M. A. 1993, ApJS, 88, 415 (Paper I)
Ryder, S. D., Staveley-Smith, L., Malin, D. F., & Walsh, W. 1994, in preparation
Sanders, R. H. 1979, in IAU Symp. 84: The Large-Scale Characteristics of the Galaxy, ed. W. B. Burton (Dordrecht: Reidel), 383
Savage, B. D., & Mathis, J. S. 1979, ARA&A, 17, 73
Schombert, J. M., & Bothun, G. D. 1987, AJ, 92, 60
Scowen, P. A., Dufour, R. J., & Hester, J. J. 1992, AJ, 104, 92
Seiden, P. E., Schulman, L. S., & Elmegreen, B. G. 1984, ApJ, 282, 95
Smith, H. E. 1975, ApJ, 199, 591
Sommer-Larsen, J., & Yoshii, Y. 1989, MNRAS, 238, 133
———. 1990, MNRAS, 243, 468
Tully, R. B. 1988, Nearby Galaxies Catalogue (Cambridge: Cambridge Univ. Press)
Twarog, B. A. 1980, ApJ, 242, 242
Walterbos, R. A. M. 1991, in IAU Symp. 144: The Interstellar Disk-Halo Connection in Galaxies, ed. H. Bloemen (Dordrecht: Kluwer), 223
Walterbos, R. A. M., & Kennicutt, R. C. 1988, A&A, 198, 61
Wang, Z. 1990a, ApJ, 360, 529
———. 1990b, ApJ, 360, 543
Warmels, R. H. 1988a, A&AS, 72, 427
———. 1988b, A&AS, 73, 453
Wevers, B. M. H. R. 1984, Ph.D. thesis, Univ. Groningen (W84)
Wyse, R. F. G. 1986, ApJ, 311, L41
Wyse, R. F. G., & Silk, J. 1987, ApJ, 313, L11
Young, J. S., & Knezek, P. M. 1989, ApJ, 347, L55
Zaritsky, D. 1992, ApJ, 390, L73